Fuel Processing Technology 287 (2026) 108450

Contents lists available at ScienceDirect

Fuel Processing Technology

journal homepage: www.elsevier.com/locate/fuproc

Pre-treatment of acidic crude palm oil using trickle bed reactor packed with polyethylene-activated carbon hybrid support

Prabakaran Uthamaseelan [a], Adeeb Hayyan [a,b,*], Mahar Diana Hamid [a,b,*], Khalid M. Abed [c,d], Jehad Saleh [e], Barun Kumar Chakrabarti [f], Bhaskar Sen Gupta [g], Wan Jefrey Basirun [h,i], Zulhelmi Amir [a,b], M. Zulhaziman M. Salleh [j], Yousef Mohammed Alanazi [e,*]

[a] Department of Chemical Engineering, Faculty of Engineering, Universiti Malaya, Kuala Lumpur 50603, Malaysia
[b] Sustainable Process Engineering Centre (SPEC), Faculty of Engineering, Universiti Malaya, 50603 Kuala Lumpur, Malaysia
[c] Department of Chemical Engineering, College of Engineering, University of Baghdad, Baghdad, Iraq
[d] Faculty of Chemical and Process Engineering Technology, Universiti Malaysia Pahang Al-Sultan Abdullah, Lebuh Persiaran Tun Khalil Yaakob, 26300 Kuantan, Pahang, Malaysia
[e] Department of Chemical Engineering, College of Engineering, King Saud University, P.O. Box 800, Riyadh 11421, Saudi Arabia
[f] Sabanci University Nanotechnology Research and Application Centre (SUNUM), Orta Mah. Üniversite Cad. No: 27/1, 34956 Tuzla, İstanbul, Turkey
[g] Institute of Infrastructure and Environment, School of Energy, Geoscience, Infrastructure and Society, Heriot-Watt University, Edinburgh EH14 4AS, United Kingdom
[h] Nanotechnology and Catalysis Research (NanoCat), Institute of Advanced Studies (IAS), Universiti Malaya, 50603 Kuala Lumpur, Malaysia
[i] Department of Chemistry, Faculty of Science, Universiti Malaya, 50603 Kuala Lumpur, Malaysia
[j] Department of Chemical and Process Engineering, Faculty of Engineering and Built Environment, Universiti Kebangsaan Malaysia, 43600 Bangi, Selangor, Malaysia

ARTICLE INFO

Keywords:
Esterification
Free fatty acid
Trickle bed reactor
4-ethylbenzenesulfonic acid
Low-density polyethylene
Wetting efficiency

ABSTRACT

A novel approach for the esterification of free fatty acid (FFA) in acidic crude palm oil (ACPO) was investigated using a trickle bed reactor (TBR). The TBR was packed with 4-ethylbenzenesulfonic acid (EBSA) supported on a low-density polyethylene (LDPE) and activated carbon (AC) hybrid support. This study introduces the use of a polyethylene-activated carbon hybrid supported catalyst in continuous TBR system which is not explored in the past research of FFA esterification. ACPO with an FFA content of 10.17 wt% was fed counter-currently with methanol vapor through the catalyst bed. Under optimum conditions, the EBSA supported on AC (EBSA/AC) achieved 92.40% FFA conversion and was successfully recycled for 3 times while the EBSA supported on LDPE:AC (1:1 mass ratio) achieved 90.20% and was recycled for once. The optimum conditions for both supported catalysts were 14 g of EBSA impregnated onto 6 g of supports, oil flow rate of 3 mL/min, 50 mL of methanol fed to the reboiler, reaction temperature of 65 °C and reaction time of 30 mins. The EBSA/AC showed a catalyst consumption of 42.50 mg/g, while the EBSA/LDPE:AC(1:1) which had 3 g of LDPE and 3 g of AC consumed 85.00 mg/g. The EBSA/AC also produced twice of the yield of treated oil compared to the EBSA/LDPE:AC(1:1). Hydrodynamic analysis indicated that the TBR operated under a trickle flow regime. The catalyst wetting efficiencies of EBSA/AC and EBSA/LDPE:AC(1:1) were 71.70% and 57.59% respectively, suggesting partial catalyst wetting in both cases. While EBSA/AC demonstrated superior performance, this study highlights the feasibility and potential utilization of polyethylene-activated carbon hybrid supported catalyst in continuous FFA esterification.

1. Introduction

Crude palm oil (CPO) extracted from palm oil mesocarp consists of both unsaturated (primarily oleic) and saturated (primarily palmitic) fatty acids [1,2]. Besides glycerides, CPO also contains minor non-glyceride compounds such as free fatty acid (FFA), metal contaminants, impurities and moisture [3]. The FFA content increases through hydrolysis by microbial lipase in the CPO. Long-term storage of harvested palm bunches, fruit bruising, microbial contamination and inefficient transportation to the mill increase the lipase activity [4]. The FFA content in CPO is undesirable since it causes a higher product loss during refining, reduces the oil stability and increases the oil rancidity

* Corresponding authors.
E-mail addresses: adeeb.hayyan@yahoo.com (A. Hayyan), mahar.diana@um.edu.my (M.D. Hamid), yalanazi1@ksu.edu.sa (Y.M. Alanazi).

https://doi.org/10.1016/j.fuproc.2026.108450
Received 8 February 2026; Received in revised form 21 March 2026; Accepted 30 March 2026
Available online 24 April 2026

[5]. Based on the Department of Standards Malaysia (DOSM), the Malaysian Palm Oil Board (MPOB) sets the maximum FFA content in CPO as 5 wt% to ensure its quality. Therefore, only CPO that meets the MPOB's standard is accepted by the Palm Oil Refiners Association of Malaysia (PORAM) to further refine for food applications [4]. This leads to a larger generation of low-grade palm oil (LGPO) in the palm oil mills.

LGPO such as acidic crude palm oil (ACPO) and sludge palm oil (SPO) contain more than 5 wt% of FFA [6]. The ACPO is a non-edible grade oil recovered from overripe fruit bunches while the SPO is the residual oil from palm oil mill effluent (POME). Generally, ACPO has an FFA content from 5 to 20 wt%, while the SPO has an FFA content that ranges from 20 to 80 wt% [7,8]. Despite being unsuitable for food applications, these by-products are promising feedstocks for biodiesel production if they undergo pre-treatment processes to reduce their FFA levels.

The pre-treatment process of LGPO is crucial for biodiesel production as FFA reacts with the base catalyst used in transesterification process to form soap, thereby resulting in a reduced catalyst efficiency [9]. Various pre-treatment techniques for FFA reduction have been explored, including chemical esterification, enzymatic methods, molecular distillation, supercritical extraction and glycerolysis [10–12].

The acid-catalyzed esterification of FFA is typically utilized for FFA reduction as it requires mild temperatures and atmospheric conditions, which lowers the operational costs and energy consumption when compared to other techniques [13]. The mechanism of acid-catalyzed FFA esterification involves four steps as presented in Fig. 1. In Step 1, a carbocation is formed after the acid catalyst's proton (H^+) protonates the carbonyl group of the FFA. The typical catalyst for esterification is sulphuric acid or sulphonic based catalyst such as p-toluenesulfonic acid and benzenesulfonic acid. In Step 2, methanol which acts as a nucleophile attacks the electrophilic carbocation and forms a tetrahedral intermediate. Fatty acid methyl ester (FAME) is formed after the intermediate rearranges itself and releases a water molecule and a proton in Step 3 and 4, respectively [14,15].

Previous studies on the FFA esterification have been based on homogenous catalysts within batch reactors. Although they have resulted in high FFA conversions due to a higher access to the active sites of homogeneous catalyst along with a longer residence time, there are some disadvantages such as insufficient catalyst separation from the product, higher catalyst consumption and longer reaction times [16,17]. To overcome these drawbacks, this study explores the application of a three-phase catalytic continuous reactor with a supported catalyst, to achieve higher FFA reduction, shorter reaction time and lower catalyst consumption.

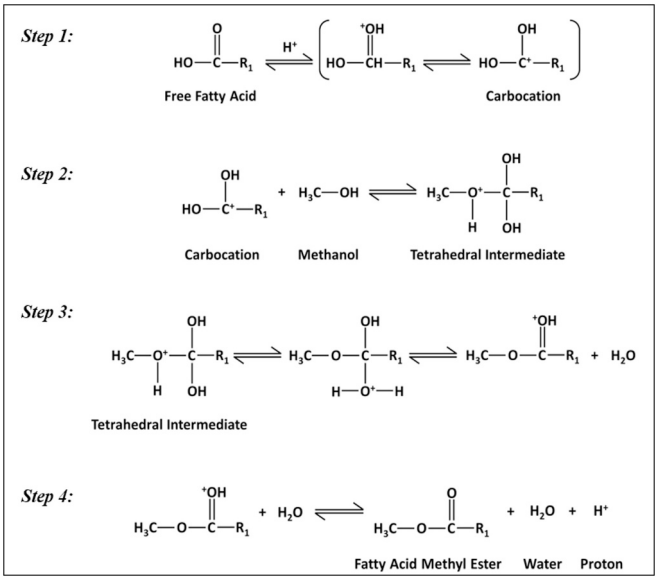

Fig. 1. The mechanism of an acid-catalyzed FFA esterification reaction.

Three-phase catalytic reactors such as fixed bed reactor (FBR) and trickle bed reactor (TBR) can be considered for FFA esterification since they are widely used in the transesterification process. While FBR is used for low viscous feed such as canola oil, soybean oil and rapeseed oil, TBR is used for high viscous feed such as crude palm oil [18–20]. Moreover, TBRs are the most commonly utilized three-phase catalytic reactors in the petrochemical industries and several studies on TBR have been reported such as the transesterification of palm oil using calcium oxide catalyst [21], esterification of acetic acid using Purolite 151 (acidic ion exchange resin) [22], hydrogenation of C_6 – C_8 olefins using cobalt-molybdenum catalyst supported on alumina [23] and hydrotreatment (hydrodesulfurization, hydrodenitrogenation and hydrodearomatization) of petroleum feed stocks [24].

TBR is selected over FBR in this study mainly due to the usage of high viscous feed which is ACPO. Since highly viscous oil flows in the form of droplets, the continuous gas flow promotes uniform liquid distribution by providing drag forces which push the viscous liquid droplets into the catalyst bed and increases the spread of liquid film over the catalyst surface. This increases the utilization of catalyst where the catalyst wetting and residence time of the liquid phase in the bed increase, thus achieving a higher mass transfer and reaction conversion in the TBR [25]. In the FBR where liquid flow is continuous, channeling of the flow could occur as highly viscous liquid has higher resistance and flows in the path with the lowest resistance. This leads to an uneven distribution of the liquid and part of the liquid phase will bypass the catalyst bed leading to a lower catalyst utilization and the distribution worsens at higher liquid velocity where the flow becomes turbulent. Moreover, the concentrated liquid flow in the channels can form hotspots and lead to thermal degradation of the catalyst [26]. Hence, a strict control over the feed flow rate is necessary for the FBR while the TBR is more adaptable to fluctuations in the feed flow rate. Higher conversion and selectivity are also achievable in TBR as the plug flow conditions are easily achieved due to the trickling flow of the liquid. Plug flow condition represents minimal axial mixing, uniform velocity profile and shorter residence time across the reactor's cross section [27]. Since the trickle flow profile typically maintains between the laminar and the transitional flow profiles, the plug flow condition is easily achieved as turbulent flow is less common in TBR.

A critical factor in the TBR performance is the catalyst design. Supported heterogeneous catalysts have significantly larger surface areas than unsupported catalysts which possess surface areas between 1 and 50 m^2/g. Examples of common catalyst supports with high specific surface area are alumina (179–497 m^2/g), silica (~750 m^2/g), and activated carbon (~830 m^2/g) [28–30]. The increased specific areas in the supports allow for the widespread dispersion of small catalyst particles, accelerating the catalytic reaction rate [31]. Additionally, the catalyst supports allow full utilization of the catalyst's efficiency as a catalytically active center. Recent studies are mainly focused on the fabrication of biochar and activated carbon (AC) from lignocellulosic biomass-based precursors from agricultural wastes such as coconut shells, rice husk and palm kernel shells [32]. AC is more expensive than biochar since it requires an additional activation step but the catalytic performance of supported catalyst using AC can be enhanced due to its larger surface area. Younghyun Lee reported 1,4-butanediol production using a Ru—Re catalyst, where the Ru–Re/biochar had 17 times lower metal dispersion on the surface in comparison to Ru–Re/AC due to the lower surface area of biochar than AC [33]. This shows the superiority of AC as catalyst support. Nagireddi also reported that AC showed greater adsorption capability of contaminants than biochar where AC adsorbed 4–10% more polychlorinated biphenyls from sediments. AC also removed bichlorinated dibenzo-p-dioxins/dibenzofurans from soil and mercury from wastewater more efficiently than biochar. Greater adsorption of AC were significantly contributed due to its finer particle size, higher porosity and surface area [34]. Hence, AC is selected as one

of the catalyst support in this study.

In addition to AC, plastic wastes are recently being studied as catalyst supports due to the plastic waste problem that has become a significant concern with a detrimental impact on both the environment and socioeconomic development. Poor management of plastic waste pollutants in the environment and significant loss in economic value are due to the plastic waste accumulation in dumps and drainages instead of being reused for a better purpose [35–37]. The development of plastic based catalytic support ensures the quality of sustainable environment and reduces the amount of plastic wastes [38,39]. The major advantages of plastic catalyst supports are their cheaper price and high mechanical strength [40]. Application of plastic as catalyst support includes photodegradation of pesticide 4-chlorophenol [38], Photo-Fenton process of Ponceau 4R dye [41], epoxidation of cinnamyl alcohol [40] and denitrification of water [42].

Several studies on biochar filled high-density polyethylene [43], biochar microsphere-polylactic acid composite [44] and polylactic acid-carbon quantum dots composite [45] showed that carbon-base materials integrated with polymer composites have stronger thermal and mechanical properties. For instance, carbon quantum dots (CQD) have been incorporated into polylactic acid (PLA) films to simultaneously improve mechanical, thermal, and degradation properties, showing that nanoscale carbon fillers can strengthen polymer matrices and accelerate degradation process [45]. Similarly, fully biomass-derived nanocomposite films fabricated from CQD and carbon nanosheet (CNS) derived from cellulose nanofiber (CNF) and or exhibited excellent mechanical strength and thermal conductivity while maintaining biodegradability [46]. Additionally, the design of all-biomass nanocomposite films for thermal management and electromagnetic interference shielding further highlights the potential of combining carbon-based materials with flexible polymeric networks to achieve multifunctional performance [47]. These studies collectively illustrate that carbon materials, when combined with polymer supports, can improve structural, thermal, and functional properties, which conceptually supports the strategy of using AC with plastic in our TBR system. As of now, there are no studies that have used AC hybridized with plastic as catalyst support for FFA esterification using TBR.

This study is particularly relevant to sustainable FFA esterification process by simultaneously addressing applications of TBR and polyethylene-activated carbon hybrid supports in a three-phase catalytic system. Objective of this study is to investigate the feasibility of using this hybrid catalyst support for the esterification of FFA in TBR. This is the first study to introduce the use of low-density polyethylene (LDPE) with AC as a hybrid packing bed in TBR for FFA esterification.

2. Experimental methods

2.1. Materials

Acidic crude palm oil was collected from a local palm oil mill in Selangor, methanol (99.8%), 4-ethylbenzenesulfonic acid ($C_8H_{10}O_3S$, 99%), granular activated carbon (AC) and low-density polyethylene (LDPE) pellets were purchased from MeRCK Malaysia Sdn. Bhd. (MeRCK). Characterization and fatty acid composition of ACPO are presented in Table 1 and Table 2 respectively. (See Table 3.)

According to MeRCK, molecular weight and density of granular AC are reported as 12.01 g/mol and 1.9 g/cm^3 respectively. Additionally, our surface morphology study revealed that the BET surface area and micropore volume of AC are 120.35 m^2/g and 0.05 cm^3/g respectively. On the other hand, MeRCK also reported that the density and melting point of white LDPE pellets are 0.925 g/mL and 116 °C respectively.

2.2. Preparation of supported acid catalyst

Despite certain changes to the supported catalyst's synthesis process, the preparation steps were mainly based on wet impregnation technique reported by Yassaghi and Davoodnia [48]. In this study, silica used by Yassaghi was replaced with LDPE, AC, and their mixtures. Firstly, the desired amounts of 4-ethylbenzenesulfonic acid (EBSA) were poured into a 250 mL conical flask and weighed on a mass balance. The EBSA was then heated at 70 °C and stirred at 300 rpm simultaneously for 10 mins on a hotplate magnetic stirrer to completely melt the excess solid lumps of acid. Five different supports were prepared by varying the mixing mass ratio of LDPE and AC. The LDPE:AC mixtures were placed in a crucible and heated at LDPE's melting point (120 °C) in a drying oven [41]. This is to allow the softened polymer to encapsulate and bind to the AC particles. This melt-blending approach establishes physical adhesion between the LDPE and AC without the use of solvents. Then, impregnation began by firstly adding supports, LDPE, LDPE:AC(2:1), LDPE:AC(1:1), LDPE:AC(1:2) and AC separately into the liquid EBSA. Methanol was then added as a co-solvent until it slightly exceeded the level of the acid-support mixtures. The mixtures were shaken for 1 h at 180 rpm using an orbital shaker. Then, the mixtures were submerged in ultrasonic water bath for 1 h to allow the adsorption of EBSA onto the supports. Finally, the wet mixtures were dried overnight at 65 °C in a drying oven to fully evaporate the methanol. The solid products were then gently crushed to obtain a uniform particle size distribution between 1.0 and 1.8 mm for further use in this study.

Table 1
Characterization of ACPO.

Parameters	Value
Free fatty acid, FFA (wt%)	10.17
Deterioration of bleachability index, DOBI	0.6
UV absorbance @ 233 nm, E233	2.35
UV absorbance @ 269 nm, E269	1.10
Peroxide value (meq O_2/kg oil)	7.9
Anisidine value	18.0
UV total oxidation value, UV Totox	3.33
Impurities (wt%)	0.02
Moisture content (wt%)	0.62
Iodine value (g I_2/100 g oil)	52.3
Saponification value (mg KOH/g oil)	192
Carotene (ppm)	251
Iron (ppm)	33.5
Copper (ppm)	0.22
Phosphorus (ppm)	11.86

Table 2
Fatty acid composition of ACPO.

Fatty Acids	Type of fatty acid	Fatty acid composition (%)
Lauric acid, C12:0	Saturated	0.112
Myristic acid, C14:0	Saturated	0.977
Palmitic acid, C16:0	Saturated	44.246
Palmitoleic acid, C16:1	Unsaturated	0.210
Stearic acid, C18:0	Saturated	4.378
Oleic acid, C18:1	Unsaturated	39.555
Linoleic acid, C18:2	Unsaturated	9.589
α-Linolenic acid, C18:3	Unsaturated	0.326
Arachidic acid, C20:0	Saturated	0.606

Table 3
FFA conversion in co-current and counter-current mode.

Flow Mode	Initial FFA (wt %)	Final FFA (wt %)	Average FFA Conversion (%)
Co-current	10.17	5.09 ± 0.55	50.00
Counter-current	10.17	3.54 ± 0.55	65.22

2.3. Reaction apparatus, experimental assays and analytical procedures

A laboratory scale TBR has been fabricated, and it primarily consists of cylindrical packing columns from stainless steel [the pilot-scale unit is displayed in Fig. 2 (a)]. The bed column consists of three sub-packing columns as shown in Fig. 2 (b). Each sub-column has a volume of 110 cm^3 where the diameter and height are 3.65 cm and 10.5 cm, respectively. The direct packing of supported catalyst in the bed column could obstruct the proper flow of reactants due to the small sizes and voids between the catalysts. Thus, polystyrene pellets have been used along with the supported catalyst. In the co-current mode, two peristaltic pumps feed the liquid methanol and ACPO into the TBR, and a distributor directs them onto the solid catalyst bed. In contrast, the liquid methanol is fed into the reboiler of TBR and vaporized during the counter-current mode. The methanol vapor then flows upward through the solid catalyst bed while the ACPO keeps flowing downward. The esterification of FFA takes place in both modes when the reactants are in constant contact with each other on the catalyst's surface. The TBR is connected to a refrigerated water bath integrated with an immersion thermostat, where its function is to circulate hot water within the jackets of the reboiler and the column. The TBR is also equipped with temperature indicators which measure the temperature of the heating jackets of both TBR column and reboiler. Besides vaporizing methanol, the reboiler also stores the product and can be drained out through the drain valve at the bottom of the reboiler. Furthermore, a reflux condenser is connected to the top of the TBR to condense the unreacted methanol vapor and circulate it into the reboiler.

To determine the suitable operating mode (co-current or counter-current flow of reactants), the fixed variables were the amount of EBSA (10 g), the amount of LDPE (10 g), ACPO flow rate (1 mL/min), reaction temperature (65 °C) and duration of run (30 mins). Only the flow direction of methanol was controlled. For the co-current mode, methanol was pumped at 2.5 mL/min while in the counter-current mode, 75 mL of methanol was fed to the reboiler and vaporized.

Based on these results, the counter-current mode was selected, and the experimental duration was fixed at 30 mins throughout the optimization process. The effects of operating parameters such as the amount of EBSA catalyst (6–18 g), the amount of catalyst support (4–12 g), the flow rate of ACPO (1–5 mL/min), the volume of methanol fed to reboiler (50–140 mL) and the reaction temperature (65–85 °C), were investigated through a single factor optimization. Note that all experiments had 3 replications, and the average values with their standard deviations were reported to ensure reproducibility and minimize experimental error. Furthermore, a one-way ANOVA analysis was presented at the end of single factor optimization. Although the MPOB's maximum limit is 5 wt% FFA, the maximum limit was restricted to 2 wt % FFA in this study. Recyclability study was performed to determine the catalytic activity, where the maximum time taken to exceed the 5 wt% limit was determined.

The main product of treated ACPO, comes along with the unreacted methanol and contains FAME, water and some escaped catalyst particles in smaller fractions. The treated ACPO was centrifuged for 4 mins at 1200 rpm. Two distinct layers were formed after centrifugation, with methanol occupying most of the lower density layer. The methanol layer was removed using a pipette. The product was further dried in a drying oven at 90 °C for 3 h to remove the moisture. The FFA content can be measured once the treated ACPO is fully cooled to room temperature.

Acid-base titration using phenolphthalein as indicator was used to calculate the FFA content in the ACPO and the treated oil. Titration technique and FFA calculation conform to the American Oil Chemist Society's (AOCS) method, Ca 5a-40, which is appropriate for commercial fats and oils. 1 g of oil sample was mixed with 50 mL of phenolphthalein

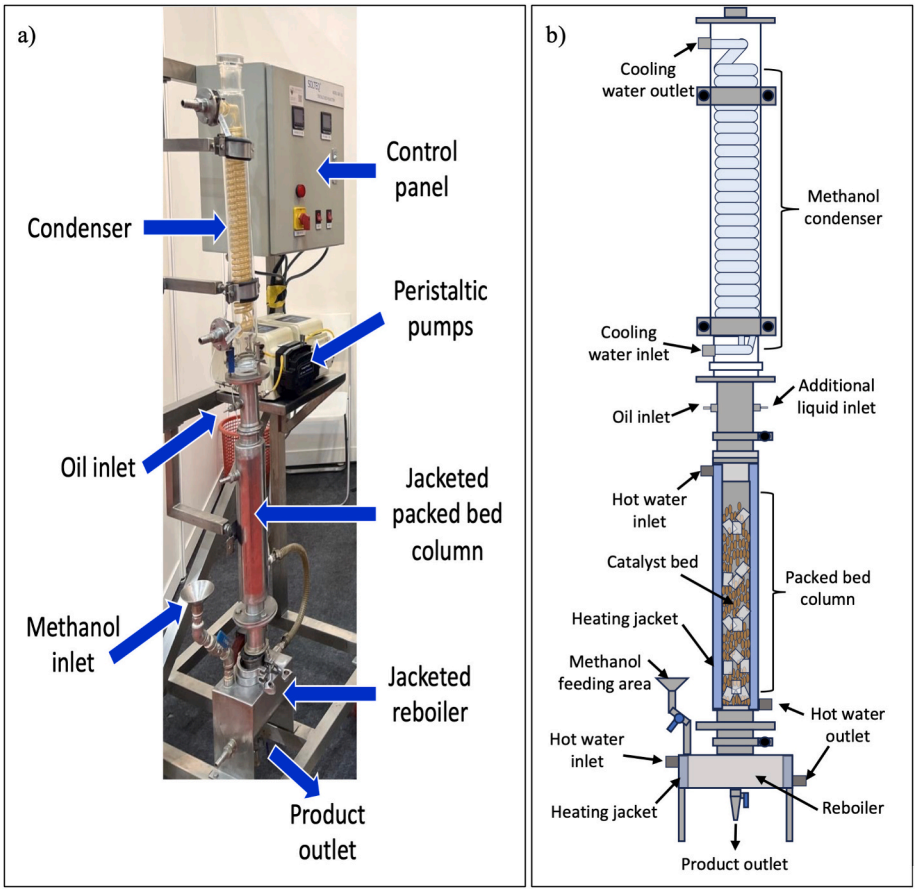

Fig. 2. Laboratory scale TBR in the pilot lab (a); Drawing of the laboratory scale TBR (b).

solution, and the mixture was titrated with potassium hydroxide (KOH) until the yellowish mixture turned reddish orange.

Eq. 1 below was used to calculate the FFA conversion:

$$\text{FFA conversion}\ (\%) = \frac{\text{FFA}_{\text{final}} - \text{FFA}_{\text{initial}}}{\text{FFA}_{\text{initial}}} \times 100\% \quad (1)$$

where,$\text{FFA}_{\text{initial}}$ is the initial FFA content (wt%) and $\text{FFA}_{\text{final}}$ is the final FFA content in treated ACPO (wt%).

Eq. 2 was used to determine the catalyst consumption, which is the mass of catalyst used per gram of the treated oil produced at the end of catalyst reusability study.

$$\text{Catalyst consumption}\left(\frac{\text{mg}}{\text{g}}\right) = \frac{\text{m}_{\text{catalyst}}}{\text{m}_{\text{treated ACPO}}} \times 100\% \quad (2)$$

where,$\text{m}_{\text{catalyst}}$ is the mass of catalyst used (mg) and $\text{m}_{\text{treated ACPO}}$ is the mass of treated ACPO (g).

2.4. Characterization of supported acid catalysts

The surface morphology of the supported catalysts were investigated using Field Emission Scanning Electron Microscope (FESEM, Model: FEI Quanta FEG 650) after the optimization study. The presence of sulfonic acid (SO_3H) which serves as a proton donor group in the EBSA catalyst, was confirmed by Energy Dispersive X-Ray (EDX) analysis incorporated with the FESEM.

2.5. Nuclear Magnetic Resonance (NMR) analysis

Nuclear magnetic resonance (NMR) spectroscopy is necessary to confirm the conversion of FFA into FAME. The spectroscopy was conducted based on Lisa and Annaliese where 20 mg of treated oil sample was dissolved in 1 mL of deutrated chloroform and transferred to 5 mm NMR tube [49]. Tetramethylsilane was used as an internal reference and the chemical shifts were reported in parts per million (ppm). Signal averaging was done by accumulating 16 scans. The ^{1}H NMR spectrum was analysed to identify characteristic peaks corresponding to functional groups of FAME.

2.6. Hydrodynamics study

The hydrodynamic parameters in TBR are important as its efficiency is heavily affected by the flow patterns of liquid and gaseous reactants through the packed bed. There are several hydrodynamic parameters that determine the TBR's efficiency such as the flow regime, pressure drop, liquid holdup, catalyst wetting efficiency, gas-liquid mass transfer coefficient, liquid-solid mass transfer coefficient and gas-solid mass transfer coefficient. Proper understanding of hydrodynamics ensures uniform distribution of reactants, sufficient contact time between the reactants and the catalyst, utilization of catalyst and overall reaction kinetics. In this study, the flow regime, liquid holdup, catalyst wetting efficiency, gas-liquid, liquid-solid and gas-solid mass transfer coefficients will be determined for the optimized conditions. Pressure changes were assumed negligible since the TBR is operating under atmospheric conditions with a short length of bed (10.5 cm).

3. Results and discussions

3.1. Mode selection of reactant flow

For the co-current mode, the FFA content was reduced from 10.17 wt % to 5.09 ± 0.55 wt% under the following conditions: 10 g of EBSA catalyst, 10 g of LDPE support, 1 mL/min of oil flow rate, 2.5 mL/min of liquid methanol flow rate, 65 °C reaction temperature and 30 mins duration run. For the counter-current mode, the FFA content was reduced from 10.17% to 3.54 ± 0.55% under the following conditions: 10 g of EBSA catalyst, 10 g of LDPE support, 1 mL/min of oil flow rate, 75 mL of methanol fed to the reboiler, 65 °C reaction temperature and 30 mins duration run. Moreover, results of one-way ANOVA test showed $F(1,4) = 11.91$ and $p = 0.03$ at 95% confidence level. This indicates mode of reactant flow significantly affect final FFA content due to $p < 0.05$.

FFA conversion for the counter-current (65.22%) was higher than the co-current mode (50.00%). This is due to the presence of oil in trickle flow which possesses larger contact area with methanol vapor in the counter-current flow compared to liquid methanol in the co-current flow. According to a study on the transesterification of sunflower oil using sodium hydroxide in a TBR by Behzadi and Farid, the conversion of sunflower oil were 95% and 99% in the co-current and counter-current modes, respectively [50]. This confirms that the heated oil and micro-sized methanol vapor droplets which flow in a counter-current mode possess larger contact surface area, thus enhancing the conversion rate. Hence, the counter-current mode was selected due to the higher FFA conversion and further optimization of operating parameters were performed in this mode.

3.2. Effect of catalyst amount

The optimization of EBSA catalyst up to 18 g is presented in Fig. 3. The fixed parameters for this step were 6 g of catalyst support, 1 mL/min of oil flow rate, 50 mL of methanol fed to the reboiler, 65 °C of reaction temperature and reaction time of 30 mins. Given the initial FFA content of 10.17 wt%, the lowest FFA content was achieved and sustained within the FFA limit of 2 wt% when 14 g of EBSA catalyst was impregnated onto the supports. The final FFA content achieved for the catalysts, EBSA/LDPE, EBSA/LDPE:AC(2:1), EBSA/LDPE:AC(1:1), EBSA/LDPE:AC(1:2) and EBSA/AC were 1.44 ± 0.55 wt%, 1.33 ± 0.44 wt%, 1.00 ± 0.44 wt %, 0.88 ± 0.33 wt% and 0.77 ± 0.22 wt%, respectively. Initially, the increase in the amount of EBSA catalyst provides more active sites for the reactants, particularly FFA and methanol to bind, thus leads to a higher reaction rate. According to a similar study on FFA esterification using sulfonated resin-polyvinyl alcohol composite (SR/PVA) in a batch reactor, SR/PVA (mass ratio 1:1) and SR/PVA (mass ratio 3:2) had FFA conversions of 78.3% and 95.0% respectively. This indicates that lack of catalytic sites in SR/PVA (mass ratio 1:1) resulted in a lower conversion [51]. Moreover, Puagsang also reported that the FFA conversion increased from 90% to 96% when the dosage of sulphuric acid catalyst was increased from 0.25% to 1.00% [7]. However, in our study, the final FFA content slightly increases (lower FFA conversion) when 16 g of EBSA catalyst was used due to the fact that an increase in the amount of EBSA catalyst beyond the optimum point leads to an excess of un-adsorbed catalyst by the support. The excess of un-adsorbed acid catalyst is more prone to leaching from the support and escapes from the bed along with the treated oil. This increases the acidity of the treated oil and results in poorer FFA conversion. Hence, the optimum amount for the EBSA catalyst is 14 g. Moreover, results of one-way ANOVA test at optimum level showed $F(4,10) = 1.48$ and $p = 0.30$ at 95% confidence level. This indicates at optimum catalyst amount (14 g), there is no significant difference between the final FFA content achieved by all five catalysts due to $p > 0.05$.

3.3. Effect of amount of catalyst support

The optimum amount of catalyst support up to 12 g is presented in Fig. 4. The fixed parameters for this step were 14 g of EBSA catalyst, oil flow rate of 1 mL/min, 50 mL of methanol fed to the reboiler, 65 °C of reaction temperature and reaction time of 30 mins. Given the initial FFA content of 10.17 wt%, the lowest FFA content was achieved and sustained within the FFA limit of 2 wt% when 6 g of catalyst support was impregnated with the EBSA catalyst. At 6 g of catalyst support, the FFA content achieved for the catalysts, EBSA/LDPE, EBSA/LDPE:AC(2:1), EBSA/LDPE:AC(1:1), EBSA/LDPE:AC(1:2) and EBSA/AC were 1.44 ±

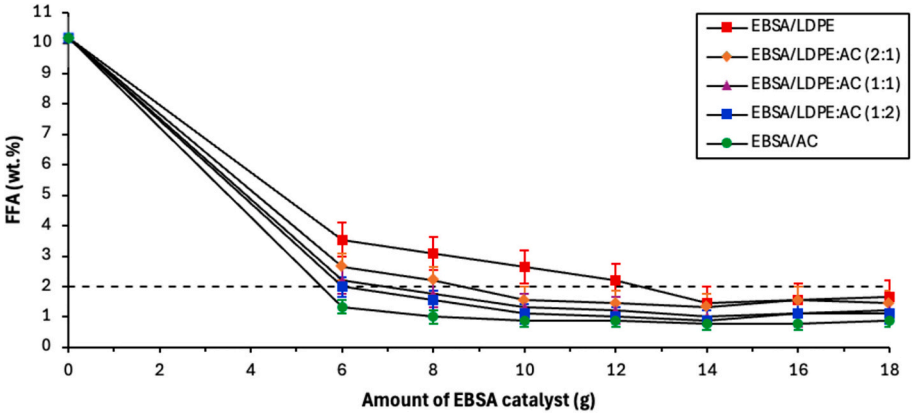

Fig. 3. Effect of EBSA catalyst amount on FFA reduction under the following conditions: 6 g of catalyst support, 1 mL/min of oil flow rate, 50 mL of methanol fed to the reboiler, 65 °C as reaction temperature & 30 mins of reaction time.

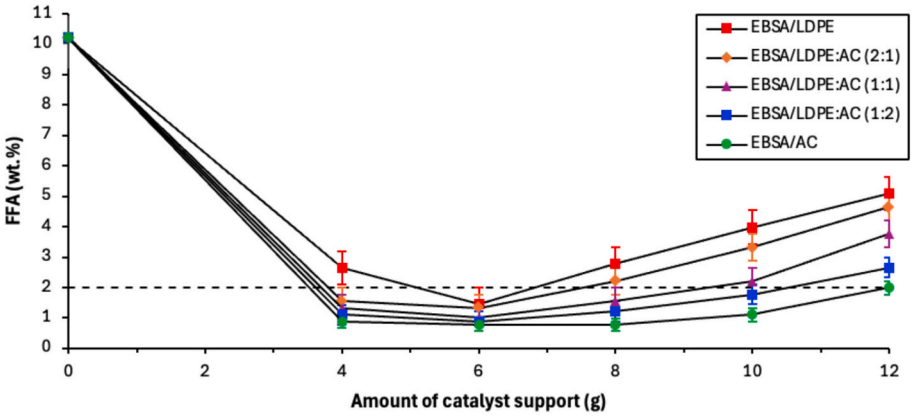

Fig. 4. Effect of catalyst support amount on the FFA reduction under the following conditions: 14 g of EBSA catalyst, 1 mL/min of oil flow rate, 50 mL of methanol fed to the reboiler, 65 °C as reaction temperature & 30 mins of reaction time.

0.55 wt%, 1.33 ± 0.44 wt%, 1.00 ± 0.44 wt%, 0.88 ± 0.33 wt% and 0.77 ± 0.22 wt%, respectively. Initially, increasing the amount of catalyst support for up to 6 g enhances the surface area for catalyst deposition, which provides larger contact area for the reactants to bind onto the active material, thus increasing the FFA reduction. However, the final FFA content was higher (lower FFA conversion) when the support amount increased to 8 g and above. Based on these observations, the increase in the support amount leads to a longer catalyst bed flow and flooding of the condensed methanol on top of the column. This inhibits the circulation of methanol vapor in the TBR system. Another possibility is the poor heat transfer within the reactor as the thickening of catalyst bed could result in hot spots which eventually reduced the reaction rate [27]. Hence, the optimum amount for the catalyst support is 6 g. Moreover, results of one-way ANOVA test at optimum level showed $F(4,10) = 1.48$ and $p = 0.30$ at 95% confidence level. This indicates at optimum support amount (6 g), there is no significant difference between the final FFA content achieved by all five catalysts due to $p > 0.05$.

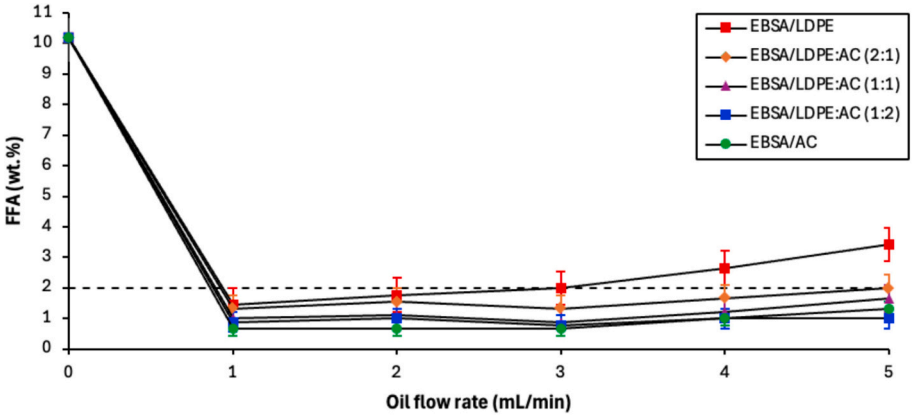

Fig. 5. The effect of oil flow rate on FFA reduction under the following conditions: 14 g of EBSA catalyst, 6 g of catalyst support, 50 mL of methanol fed to the reboiler, 65 °C as reaction temperature & 30 mins of reaction time.

3.4. Effect of oil flow rate

The optimization of the oil flow rate up to 5 mL/min is presented in Fig. 5. The fixed parameters for this step were 14 g of EBSA catalyst, 6 g of catalyst support, 50 mL of methanol fed to the reboiler, 65 °C of reaction temperature and reaction time of 30 mins. With an initial FFA content of 10.17 wt%, majority of the supported catalysts achieved the lowest FFA content and sustained within FFA limit of 2 wt% when the oil flow rate was 3 mL/min. At this flow, the FFA content of the catalysts, EBSA/LDPE, EBSA/LDPE:AC(2:1), EBSA/LDPE:AC(1:1), EBSA/LDPE:AC(1:2) and EBSA/AC were 1.99 ± 0.55 wt%, 1.33 ± 0.44 wt%, 0.88 ± 0.44 wt%, 0.77 ± 0.33 wt% and 0.66 ± 0.22 wt%, respectively. As the oil flow rate increases, larger volumes of oil could wet the catalyst particles and more FFA molecules will reach the active sites to react with methanol. Higher catalyst wetting is necessary to reduce the regions of low catalyst utilization which enhances the mass transfer of reactants towards the catalyst surface. However, the final FFA content were higher (lower FFA conversion) when the oil flow rate increased to 4 mL/min and above. This could be due to the larger oil films covering the catalyst particles that increase the mass transfer resistance of methanol vapor to the active sites thereby lowering the FFA reduction. Due to a lack of substantial research investigations on the continuous esterification of FFA, the effect of oil flow rate was compared with the transesterification of rapeseed oil using TBR by Meng and Tian. They reported that the oil conversion increased from 93% to 94% when the oil flow rate was raised from 0.1 mL/min to 0.6 mL/min. However, the oil conversion dropped significantly to 79% when the oil flow rate was further increased to 1.0 mL/min [52]. Hence, the optimum oil flow rate in our study is 3 mL/min due to the satisfactory reduction in the FFA content whilst enhancing the throughput. In addition, results of one-way ANOVA test at optimum level showed $F(4,10) = 5.28$ and $p = 0.02$ at 95% confidence level. This indicates at optimum oil flow rate (3 mL/min), there is a significant difference between the final FFA content achieved by all five catalysts due to $p < 0.05$.

3.5. Effect of methanol volume fed to the reboiler

The optimization of methanol volume fed to the reboiler until 140 mL is presented in Fig. 6. The fixed parameters for this step were 14 g of EBSA catalyst, 6 g of catalyst support, 3 mL/min of oil flow rate, and 65 °C of reaction temperature and reaction time of 30 mins. With an initial FFA content of 10.17 wt%, the lowest FFA content was achieved and sustained within the FFA limit of 2 wt% when the methanol volume was 50 mL. At this flow, the FFA content for catalysts, EBSA/LDPE, EBSA/LDPE:AC(2:1), EBSA/LDPE:AC(1:1), EBSA/LDPE:AC(1:2) and EBSA/AC were 1.99 ± 0.55 wt%, 1.33 ± 0.44 wt%, 0.88 ± 0.44 wt%, 0.77 ± 0.33 wt% and 0.66 ± 0.22 wt%, respectively. There was no significant difference when the methanol volume was increased to 80 mL. This could be attributed to the fact that a further increase in methanol concentration was ineffective owing to the coverage of oil film on the catalyst particle that limited the access of methanol to the active sites. The final FFA achieved were higher (lower FFA conversion) when the methanol volume was increased to 100 mL and above. This could be due to the higher methanol flow rate which disrupts the flow distribution of oil when operating in a counter-current mode. This lowers the catalyst wetting potential of the oil flow and thereby reduces the mass transfer of oil to the active sites of the catalyst. Owing to the limited research investigations on the continuous esterification of FFA, the effect of methanol flow rate was compared with the transesterification of sunflower oil in a TBR by Son and Kusakabe [53]. With an oil flow rate of 4.2 mL/h and reaction temperature of 100 °C, the conversion increased from 80% to 95% when the flow rate of methanol increased from 1 mL/h to 2 mL/h. However, when the flow rate was further increased to 3 mL/h, the conversion dropped from 95% to 80%. Moreover, another study by Ulfat Zia on biodiesel production using membrane reactor packed with phyto-nano catalyst showed that the product yield achieved about 75% when the methanol to oil ratio was increased to 9:1 but a decline in the yield was observed when the methanol to oil ratio was increased further to 15:1 [54]. These two studies showed similar pattern with our study. Hence, the optimum volume of methanol fed to the reboiler is 50 mL. In addition, results of one-way ANOVA test at optimum level showed $F(4,10) = 5.28$ and $p = 0.02$ at 95% confidence level. This indicates at optimum methanol volume (50 mL), there is a significant difference between the final FFA content achieved by all five catalysts due to $p < 0.05$.

3.6. Effect of reaction temperature

The optimization of reaction temperature up to 85 °C is presented in Fig. 7. The fixed parameters for this step were 14 g of EBSA catalyst, 6 g of catalyst support, oil flow rate of 3 mL/min, 50 mL of methanol fed to the reboiler and reaction time of 30 mins. With an initial FFA content of 10.17 wt% for all types of supported catalyst, the lowest FFA content was achieved and sustained within the FFA limit of 2 wt% when the reaction temperature was 65 °C. The FFA content achieved for the catalysts, EBSA/LDPE, EBSA/LDPE:AC(2:1), EBSA/LDPE:AC(1:1), EBSA/LDPE:AC(1:2) and EBSA/AC were 1.99 ± 0.55 wt%, 1.33 ± 0.44 wt%, 0.88 ± 0.44 wt%, 0.77 ± 0.33 wt% and 0.66 ± 0.22 wt%, respectively at 65 °C. When the reaction temperature was increased to 70 °C and above, the FFA content was higher, hence the FFA conversion decreased. This could be due to the increase in the methanol vapor flow rate with temperature which results in a rapid condensation of methanol that eventually inhibits the methanol vapor flow rate over time. Moreover, the polystyrene pellets used along with the supported catalyst were

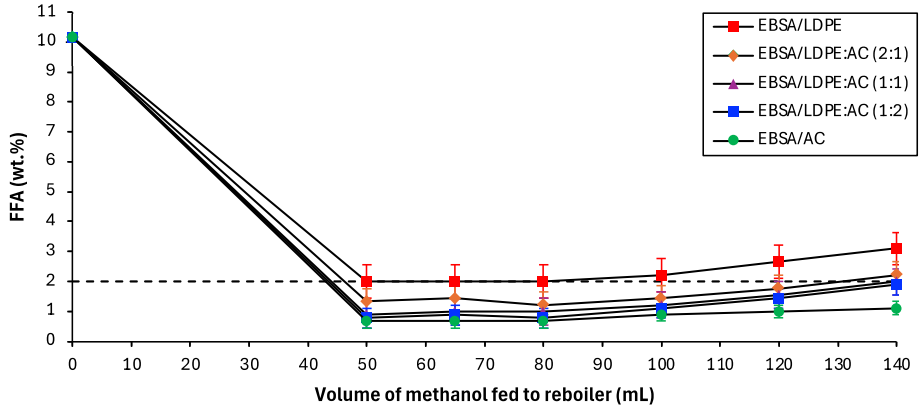

Fig. 6. Effect of methanol volume fed to reboiler on FFA reduction under the following conditions: 14 g of EBSA catalyst, 6 g of catalyst support, 3 mL/min of oil flow rate, 65 °C as reaction temperature & 30 mins of reaction time.

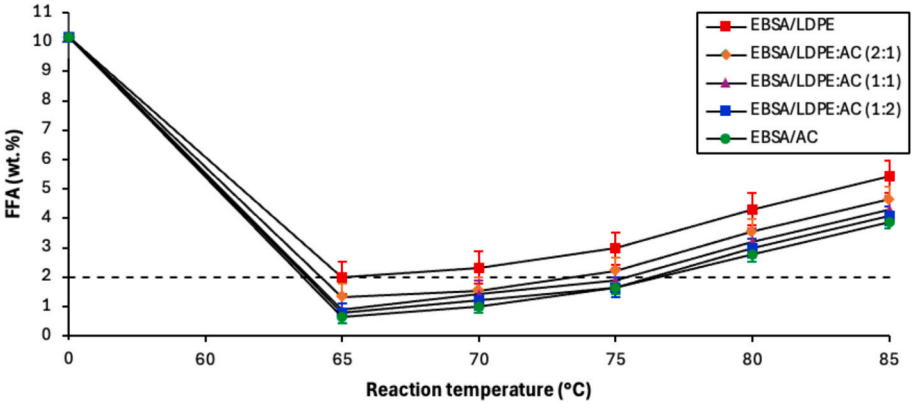

Fig. 7. Effect of reaction temperature on the FFA reduction under the following conditions: 14 g of EBSA catalyst, 6 g of catalyst support, 3 mL/min of oil flow rate, 50 mL of methanol fed to the reboiler & 30 mins of reaction time.

broken at more than 80 °C due to the thermal expansion. This disrupts the supported catalyst distribution in the packing basket. As a result, the supported catalyst escapes from the bed due to its smaller size and decreases the FFA reduction efficiency. Compared to other studies on FFA esterification using batch reactors, it was reported that the optimum reaction temperature was 60 °C to avoid methanol loss via vaporization since its boiling point is 64.7 °C [8,55,56]. However, in the case of the TBR, given the fact that are no similar studies conducted using TBRs, the methanol was vaporized at 65 °C in the system. Hence, the optimum reaction temperature is 65 °C. In addition, results of one-way ANOVA test at optimum level showed $F(4,10) = 5.28$ and $p = 0.02$ at 95% confidence level. This indicates at optimum temperature (65 °C), there is a significant difference between the final FFA content achieved by all five catalysts due to $p < 0.05$.

3.7. Effect of reaction time

The optimization of reaction time is presented in Fig. 8. The maximum time that the supported catalyst bed can be used before it loses its catalytic activity can be determined in this study. This study was performed under optimized conditions: 14 g of EBSA impregnated on 6 g of support, 3 mL/min oil flow rate, 50 mL of methanol fed to the reboiler and reaction temperature of 65 °C. To sustain a FFA content below 2 wt %, the maximum time for the supported catalysts, EBSA/LDPE, EBSA/LDPE:AC(2:1), EBSA/LDPE:AC(1:1), EBSA/LDPE:AC(1:2) and EBSA/AC were 30 mins, 30 mins, 60 mins, 90 mins and 120 mins, respectively. Firstly, the FFA content for EBSA/LDPE was sustained within 1.99 ± 0.55 wt% until 30th min. At the 60th min, the FFA content achieved was 8.40 ± 0.55 wt% which exceeded the 2 wt% target. Secondly, the FFA content using EBSA/LDPE:AC(2:1) was sustained at 1.33 ± 0.44 wt% until 30th min. At the 60th minute, the FFA content achieved was 2.43 ± 0.44 wt% which exceeded the 2 wt% target. Thirdly, the FFA content using EBSA/LDPE:AC(1:1) was sustained at 1.77 ± 0.44 wt% until 60th min. At the 90th min, the FFA content achieved was 2.65 ± 0.44 wt% which exceeded the 2 wt% target. Next, the FFA content using EBSA/LDPE:AC(1:2) was sustained at 1.88 ± 0.33 wt% until 90th min. At the 120th min, the FFA content achieved was 2.65 ± 0.33 wt% which exceeded the 2 wt% target. Lastly, the FFA content using EBSA/AC was sustained at 1.99 ± 0.22 wt% until 120th min. At the 150th min, the FFA content achieved was 2.88 ± 0.22 wt% which exceeded the 2 wt% target. This shows that the catalyst bed usage duration increases with the composition of the activated carbon in the LDPE:AC hybrid support. Hence, the catalyst supported on pure AC shows longer lifespan compared to the catalyst supported on LDPE:AC mixture and pure LDPE. This also indicates that the AC holds the EBSA catalyst stronger than the LDPE due to its higher porosity. AC possesses a large surface area and a network of pores of varying sizes, which provide more sites for the binding of the catalyst. This increased surface area allows for stronger bonding between the catalyst and the carbon surface. Organic acids such as EBSA are primarily adsorbed onto the hydrophobic sites of the AC which mainly comprises of graphene layers [57]. AC possesses functional groups such as hydroxyl, carboxyl and phenolic groups on the surface which forms strong chemical bonds with polar compounds such as sulfonic acid. In contrast, LDPE is a non-polar polymer that has low affinity towards polar compounds. However, the formation of activated carbon with LDPE as a hybrid support promotes the binding of the LDPE onto the AC surface through the weak Van der Waals forces and improves the EBSA catalyst adsorption compared to pristine LDPE.

3.8. Recyclability study

Based on the maximum time limit to sustain the FFA content within 2 wt%, the number of experimental runs and catalyst consumption can be determined and are presented in Table 4. EBSA/AC achieved the

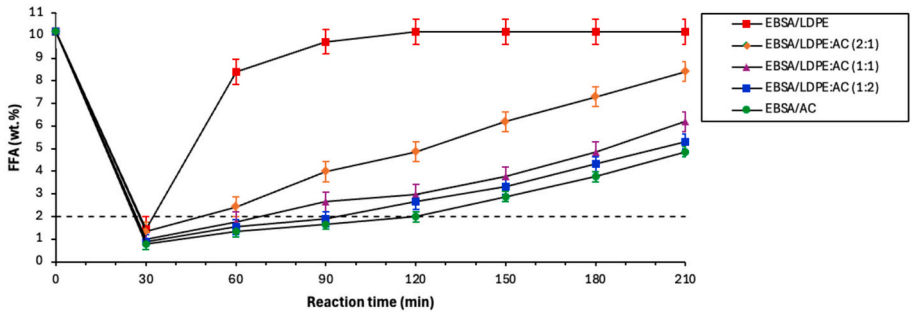

Fig. 8. Effect of reaction time on FFA reduction under the following conditions: 14 g of EBSA catalyst, 6 g of catalyst support, 3 mL/min of oil flow rate, 50 mL of methanol fed to the reboiler & 65 °C as reaction temperature.

Table 4
Summary of recyclability study.

Supported catalyst	Number of experimental runs	Average FFA conversion (%)	Total yield of treated oil (g)
EBSA/LDPE: AC(1:1)	1	90.22	165
	2	82.61	
EBSA/LDPE: AC(1:2)	1	91.30	247
	2	84.78	
	3	81.52	
EBSA/AC	1	92.39	330
	2	86.96	
	3	83.70	
	4	80.43	

lowest catalyst consumption which was 42.50 mg EBSA/ treated oil and can be recycled for 3 times. EBSA/LDPE:AC(1:2) had a catalyst consumption of 56.67 mg EBSA/ treated oil and can be recycled for twice. The EBSA/LDPE:AC(1:1) had a catalyst consumption of 85.00 mg EBSA/ treated oil and can be recycled for once. Lastly, EBSA/LDPE:AC(2:1) and EBSA/LDPE, both had the highest catalyst consumption of 97.15 mg EBSA/ treated oil and cannot be recycled. The summary of the recyclability study is shown in Table 4 below.

3.9. Validation of optimum conditions

The EBSA catalyst supported onto LDPE:AC at different mass ratios such as 1:0, 2:1, 1:1, 1:2 and 0:1 were optimized in this study. The results showed that under counter-current mode, the EBSA/AC was the optimum mixing ratio with the highest conversion, 92.40% at 30 min of reaction time, 14 g of EBSA catalyst, 6 g of catalyst support, oil flow rate of 3 mL/min, 50 mL of methanol fed to the reboiler and reaction temperature of 65 °C. The yield of treated oil was 330 g with a catalyst consumption of 42.50 mg EBSA/ treated oil. It can be concluded that the catalyst supported on pure AC has superior results over LDPE and LDPE:AC supports. Although EBSA supported on LDPE offers an advantage for continuous water removal due to its hydrophobicity, the higher surface area and porosity of EBSA/AC were the key factors in contributing to the higher FFA conversion. EBSA/LDPE:AC(1:1) can be considered due to its plastic (LDPE) valorization. However, with a yield of 165 g and catalyst consumption of 85.00 mg EBSA/ treated oil, 50% of treated oil yield was lost in comparison with EBSA/AC. Moreover, catalyst consumption was increased by 50% for EBSA/LDPE:AC(1:1). This results indicate the limitations of LDPE application in the design of packed bed in TBR but highlights their potential use.

Table 5 below shows the comparison between our results and past studies on FFA esterification. Generally, our results were comparable although our study varies in terms of reactor type, counter-current operation and the FFA limit of 2 wt% set for recyclability study.

3.10. Characterization of supported acid catalyst

FESEM imaging and EDX analyses were used to provide topographical and elemental information of the EBSA/AC and EBSA/LDPE:AC (1:1). The FESEM images of pristine AC, EBSA/AC after reaction, and EBSA/LDPE:AC(1:1) after reaction are presented in Fig. 9. The FESEM images of the supported catalysts before reaction could not be obtained due to the limitations of high vacuum operation of the FESEM machine. Since the EBSA formed a slightly wet and reflecting layer on the catalysts before reaction, such components could not be analysed under high vacuum sustained in the chamber. However, EDX analysis presented in Fig. 10 revealed that the EBSA was well impregnated into the AC and LDPE:AC layers. Initially, the pristine AC in Fig. 10 (a) consisted of 74.4 wt% of carbon (C), 6.8 wt% of oxygen (O) with the absence of sulphur (S). However, although the supported catalysts were analysed after their maximum reusability limits, Fig. 10 (b) shows that the EBSA/AC consisted of 75.2 wt% of element C, 12.4 wt% of element O and 1.8 wt% of element S, while Fig. 10 (c), shows that the EBSA/LDPE:AC(1:1) consisted of 88.5 wt% of element C, 12.3 wt% of element O and 2.0 wt% of element S. The presence of sulfonic acid functional group (SO_3H) of EBSA contributed to the rise in elemental S for both EBSA/AC and EBSA/LDPE:AC(1:1). Moreover, the increase in element C for both supported catalysts were due to the presence of benzene ring of the EBSA. Furthermore, the presence of elemental C in the EBSA/LDPE:AC(1:1) were increased by the long chain of the ethylene monomers in the LDPE. **(a).**

Hence, the overall results showed that the EBSA was well impregnated onto the supports, AC and LDPE:AC(1:1) and could be utilized for the esterification of FFA in the TBR.

3.11. NMR results for treated oil

The ^{1}H NMR spectrum was obtained for treated oil after 1 run using EBSA/AC catalyst. As shown in Fig. 11, the peak (singlet) at 3.69 ppm represents methoxy (–OCH_3) protons of FAME which confirms the successful FFA esterification. This result aligns with a similar study by Kawarpal Singh, where the ^{1}H NMR spectrum of biodiesel exhibited a peak (singlet) at 3.57 ppm corresponding to the formation of FAME

Table 5
Comparison with past studies on FFA esterification.

No.	Reactor Type	Catalyst	Operating Conditions	Reaction Time	FFA Conversion (%)	References
1.	TBR (Counter-current mode)	EBSA/AC	• 14 g of EBSA catalyst impregnated onto 6 g AC • ACPO flow rate: 1 mL/min • Methanol Volume: 50 mL • Reaction temperature: 65 °C	120 mins	• 1st run: 92.39% • 4th run: 80.43%	–
2.	TBR (*Co*-current)	Benzenesulfonic acid-choline chloride DES/AC	• 8 g of EBSA catalyst impregnated onto 6 g AC • ACPO flow rate: 1 mL/min • Methanol flow rate: 4 mL/min • Reaction temperature: 60 °C	TBR (*Co*-current)	• 1st run: 97.50%	[58]
3.	FBR (*Co*-current mode)	Amberlyst-15	• 5 g of catalyst • Sunflower oil flow rate: 85 mL/h • Methanol flow rate: 9 mL/h • Reaction temperature: 100 °C	300 mins	• 1st run: 97.50%	[58]
4.	Batch reactor	Hydrochloric acid	• Catalyst dosage: 0.25% • Molar ratio of methanol to ACPO: 10:1 • Reaction temperature: 60 °C	120 mins	95.95%	[7]
5.	Batch reactor	Titanium oxysulphate sulphuric acid	• Catalyst dosage: 7% • Molar ratio of methanol to ACPO: 10:1 • Reaction temperature: 60 °C	120 mins	73.45%	[55]

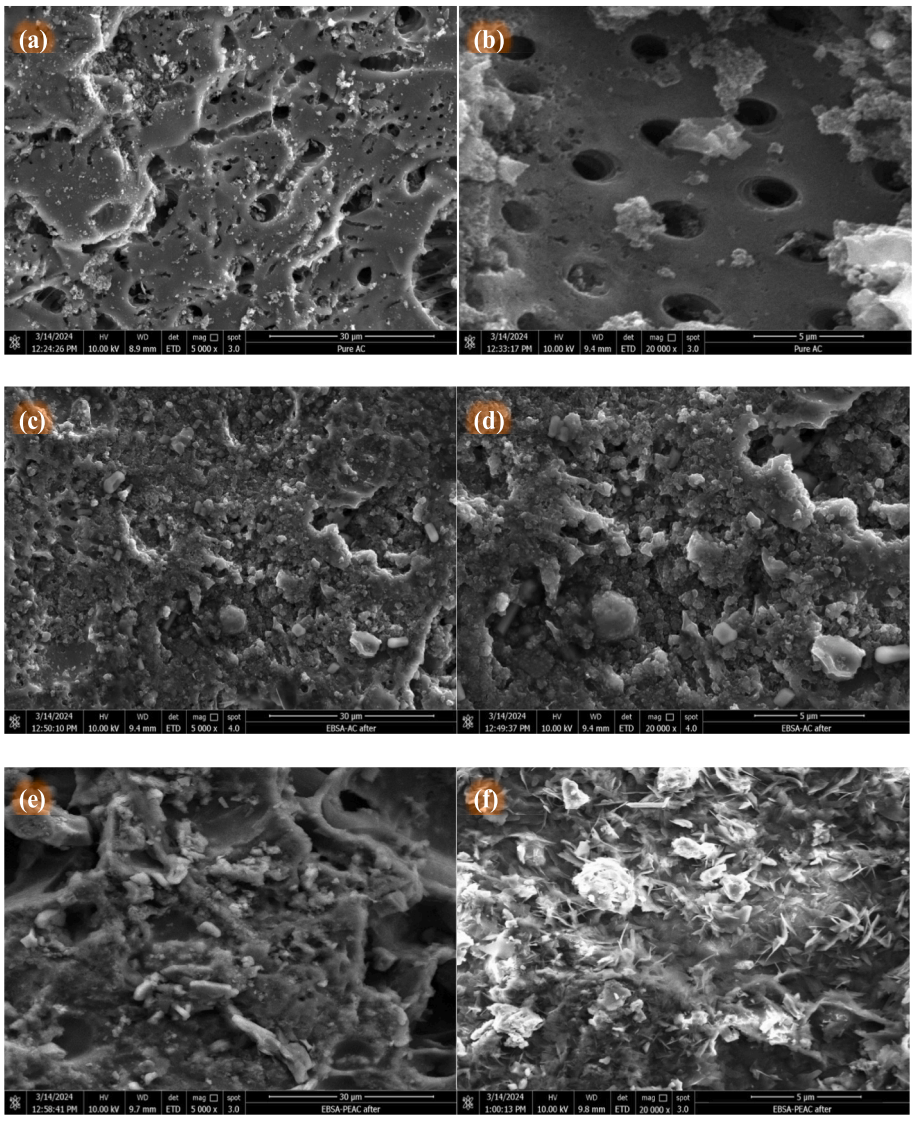

Fig. 9. FESEM imaging of pristine AC at (a) 5000 × and (b) 20,000 × magnification, EBSA/AC after reaction at (c) 5000 × and (d) 20,000 × magnification, EBSA/LDPE:AC(1:1) after reaction at (e) 5000 × and (f) 20,000 × magnification.

[59]. The appearance of ester-related signal provides further evidence of high FFA conversion (92.40%) by EBSA/AC during the first run.

3.12. Hydrodynamics study

Hydrodynamic study was conducted for EBSA/AC and EBSA/LDPE:AC(1:1) under optimum conditions which are counter-current mode, 30 min of reaction time, 14 g of EBSA catalyst, 6 g of catalyst support, oil flow rate of 3 mL/min, 50 mL of methanol fed to the reboiler and reaction temperature of 65 °C. It is important to note that the hydrodynamic parameters in this study were estimated based on the physical properties of the raw feed materials (ACPO and methanol) prior to the reaction. As esterification progresses, the viscosity reduced due to production of FAME from FFA in ACPO. The formation of FAME leads to a gradual decrease in the viscosity of the reaction mixture, which can significantly alter the rheological behavior and impact both mass transfer and hydrodynamics within TBR. Therefore, the current hydrodynamic analysis is valid primarily for the initial stage of the reaction. Further investigations are recommended to characterize and model the dynamic changes in viscosity throughout the reaction process to achieve a more comprehensive understanding of the reactor performance under actual operating conditions. Moreover, the optimized methanol volume (50 mL) fed to the reboiler was expressed as gas volumetric flow rate in this hydrodynamic study. Our calculation revealed that the time taken to vaporize 50 mL of methanol under optimum condition is 20.74 s, hence the methanol gas volumetric flow rate is 2.41 mL/s. Furthermore, all constants used to calculate the hydrodynamic parameters are presented in Table 6.

3.13. Flow regime

The flow regime is an important consideration in TBR design as it possesses a significant impact on the hydrodynamic parameters such as pressure drop, liquid holdup, wetting efficiency and mass transfer coefficients. The flow regime is influenced by parameters such as the fluid flow rates, the physical and chemical characteristics such as density [60]. The flow regimes in a TBR can be categorized into four regimes which are the trickle flow, pulse flow, spray and bubbly regimes. Charpentier and Favier proposed a flow map to identify the flow regimes in the TBR as presented in Fig. 12 [61]. The Y-axis and X-axis coordinates of the map can be determined from Eqs. 3 and 4, respectively:

$$\mathrm{Y-axis}: \frac{\mathrm{L}}{\mathrm{G}}\lambda\Psi\# \tag{3}$$

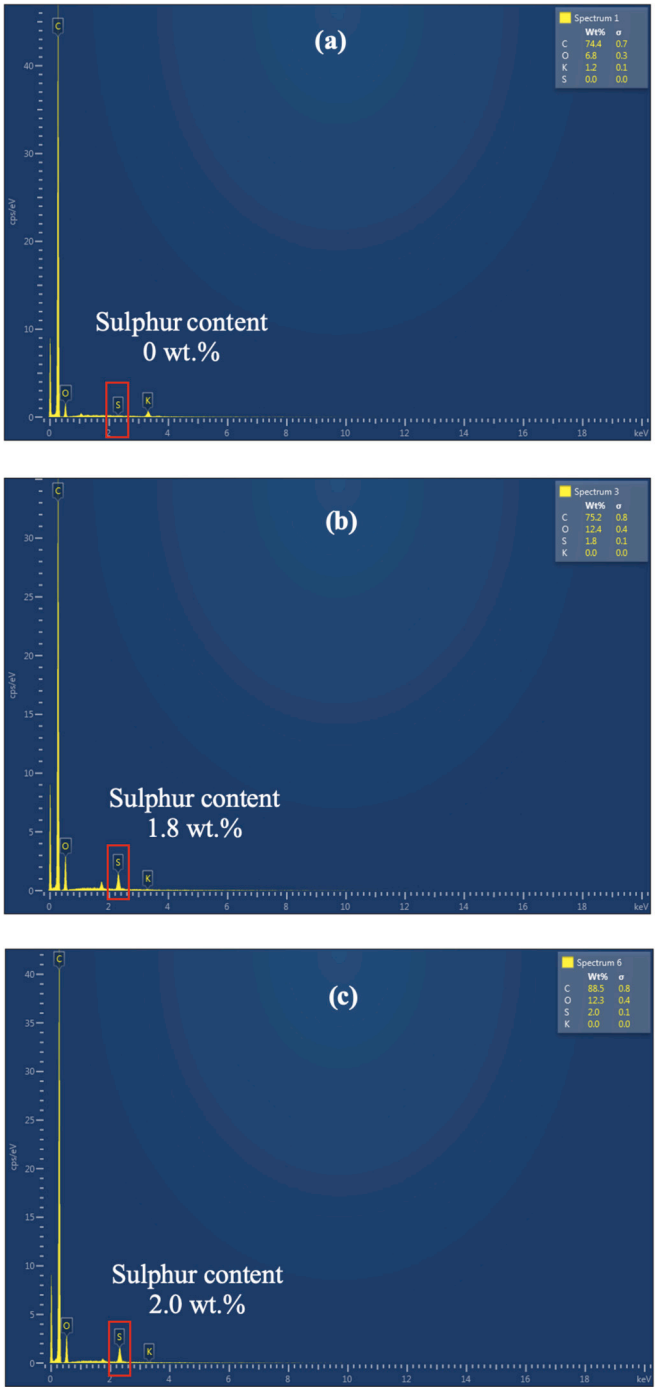

Fig. 10. EDX spectra plot of (a) pristine AC, (b) EBSA/AC supported catalyst after reaction and (c) EBSA/LDPE/AC supported catalyst after reaction.

$$X-\text{axis}: \frac{G}{\lambda}\# \tag{4}$$

where,

L is the liquid oil superficial flow rate (7.07×10^{-3} m/s) while G is the methanol gas superficial flow rate (2.30×10^{-3} m/s). λ and Ψ are the dimensionless flow parameters determined using Eq. 5 and 6, respectively [61]:

$$\lambda = \left(\frac{\rho_G}{\rho_{air}}\frac{\rho_L}{\rho_{water}}\right)^{0.5} \tag{5}$$

$$\Psi = \frac{\sigma_{water}}{\sigma_L}\left[\frac{\mu_L}{\mu_{water}}\left(\frac{\rho_{water}}{\rho_L}\right)^2\right]^{0.33} \tag{6}$$

where,

$\rho_G$is the density of methanol vapor (1.21 kg/m^3), ρ_L is the density of oil (915 kg/m^3), ρ_{air} is the density of air (1.14 kg/m^3), ρ_{water} is the density of water (997 kg/m^3), $\mu_L$is the viscosity of oil (3.67×10^{-2} Pa.s), μ_{water} is the viscosity of water (1.00×10^{-3} Pa.s), σ_L is the surface tension of oil (3.08×10^{-2} N/m) and σ_{water} is the surface tension of water (7.20×10^{-2} N/m).

Based on the calculation using Eq. 3 & 4, Charpentier-Favier chart indicates that under current optimized parameters (oil flow rate: 3 mL/min & methanol vapor flow rate: 2.41 mL/s), operating regime is at the X-axis: 0.0025, while the Y-axis: 24.58, which is under trickle flow regime (refer to blue point in Fig. 12). The gas and liquid flow in continuous and semi-continuous phases, respectively, occurs under the trickle flow regime. The partial wetting of trickle flow occurs at a very low liquid flow rate as the kinetic energy of liquid decreases and the energy is insufficient to overcome the interfacial forces at the liquid-solid interface [62]. However, at sufficiently high liquid flow rates, the wetting condition changes to complete wetting where the liquid phase completely covers the surface of the catalyst. While the trickle flow regime possesses high stability during operations, it is less suitable for mass transfer-controlled reactions due to its lower mass transfer rate than the pulse regime. Under the pulse flow regime where both liquid and gas flow semi-continuously, liquid plugs are formed when the liquid agglomerates to fill the voids between the particles. The liquid plugs at the catalyst surface are held together by the gas phase pockets that form between them and consequently, higher mass transfer rates are achieved when the visible gas and liquid-rich slugs pass through the catalysts in alternate directions.

As a result, the vast majority of industrial TBRs are operated at the boundary in between the pulse and trickle flow. In industries, TBR is generally operated at trickle-pulse transition regime for enhanced mass transfer and better catalyst utilization to boost the production capacity. However, the current laboratory TBR is restricted to the trickle flow regime due to its smaller design and consequently, the transition regime could not be achieved. This agrees well with the results of Mansour Ali that suggests that the coordinates for the laboratory/pilot TBR conforms to the trickle regime while the coordinates for the larger industrial TBRs conforms to the transition and beyond regimes [63].

3.13.1. *Liquid Holdup*

The liquid holdup in a TBR is defined as the volume of liquid per unit bed volume. Liquid holdup can be further divided into static and dynamic. Static liquid holdup refers to the volume of liquid per unit volume of bed that remains trapped in the bed after draining, whereas dynamic liquid holdup refers to the volume of liquid that flows through per unit volume of bed. The liquid holdup affects a large number of other hydrodynamic TBR parameters, such as the mass transfer coefficients and wetting efficiency. The residence time of the liquid phase and the corresponding reactant conversion depends on the liquid holdup in the bed. Therefore, it is crucial to comprehend how the structure of the reactor (column diameter, particle size, etc.) and its operating parameters (gas and liquid flow rates, fluids' physical and chemical properties, etc.) affect the liquid holdup. Eq. 7 to 9 are the correlations proposed by Wammes and Mechielsen and it shows the effect of particle diameter and liquid flow rate on the dynamic liquid holdup for low interaction regime [64]. Note that these correlations are only applicable for TBR operating at atmospheric conditions.

For the low interaction regime:

$$\text{Liquid holdup}, \beta_d = 3.8\text{Re}_L^{0.55}(\text{Ga}_L)^{-0.42}\left(\frac{6(1-\varepsilon_B)d_p}{\varepsilon_B}\right)^{0.65}\# \tag{7}$$

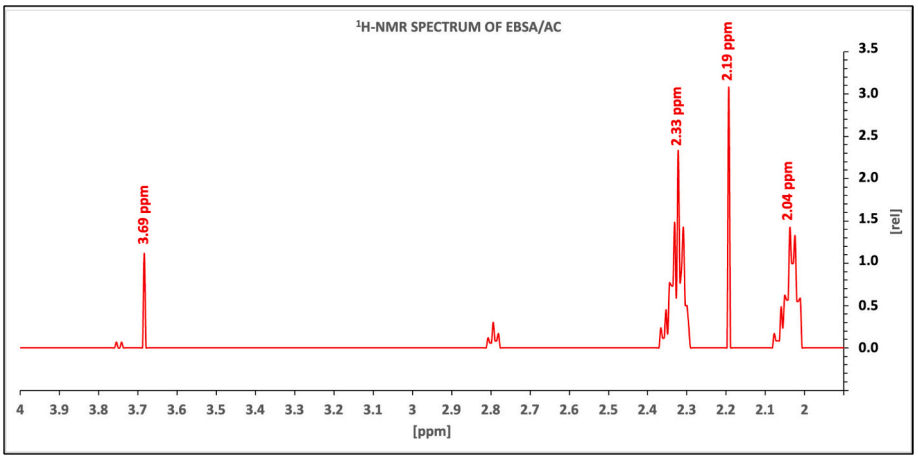

Fig. 11. ^{1}H NMR, spectrum of treated oil using EBSA/AC catalyst after 1 run.

Table 6
Constants used for hydrodynamic parameters calculation.

Item	Symbol	Value	Unit
Diameter of sub-column	D_C	3.65×10^{-2}	m
Height of sub-column	H_C	1.05×10^{-1}	m
Diameter of oil tube	D_T	3.00×10^{-3}	m
Cross section area of packing basket	A_C	1.05×10^{-3}	m^2
Volume of sub-column	V_C	1.10×10^{-4}	m^3
Cross section area of oil tube	A_T	7.07×10^{-6}	m^2
Particle diameter of EBSA/AC	$d_{p(1)}$	1.00×10^{-3}	m
BET surface area of EBSA/AC	$a_{s(1)}$	117.45	m^2/g
Porosity of EBSA/AC	ε_1	1.70×10^{-7}	m^3/g
Particle diameter of EBSA/LDPE:AC(1:1)	$d_{p(2)}$	1.80×10^{-3}	m
BET surface area of EBSA/LDPE:AC(1:1)	$a_{s(2)}$	59.15	m^2/g
Porosity of EBSA/LDPE:AC(1:1)	ε_2	9.00×10^{-8}	m^3/g
Density of methanol vapor @ 65 °C	ρ_G	1.21	kg/m^3
Density of ACPO	ρ_L	915	kg/m^3
Density of air	ρ_{air}	1.14	kg/m^3
Density of water	ρ_{water}	997	kg/m^3
Surface tension of ACPO	σ_L	3.08×10^{-2}	N/m
Surface tension of water	σ_{water}	7.20×10^{-2}	N/m
Viscosity of ACPO	μ_L	3.67×10^{-2}	Pa.s
Viscosity of water	μ_{water}	1.00×10^{-3}	Pa.s
Viscosity of methanol vapor @ 65°C	μ_G	1.14×10^{-5}	Pa.s
Gravitational acceleration	g	9.81	m/s^2
Bed porosity	ε_B	0.50	–
Diffusivity of methanol in oil	D_{AL}	6.00×10^{-7}	m^2/s
Diffusivity of methanol in air	D_{AB}	1.64×10^{-5}	m^2/s
Molecular weight of ACPO	MW_L	256	kg/kmol
Molecular weight of methanol	MW_G	32.04	kg/kmol

$$\text{Reynolds number of liquid phase, } Re_L = \frac{\rho_L L d_p}{\mu_L} \# \tag{8}$$

$$\text{Galileo number, } Ga_L = \frac{{d_p}^3 {\rho_L}^2 g}{{\mu_L}^2}\left(1 + \frac{\Delta P/Z}{\rho_L g}\right) \# \tag{9}$$

where,d_p is the particle size (EBSA/AC: 1.00×10^{-3} m; EBSA/LDPE:AC (1:1): 1.80×10^{-3} m), ε_B is the bed void (0.50), g is the gravitational acceleration (9.81 m/s^2), ρ_L is the density of oil (915 kg/m^3), $\mu_L$is the viscosity of oil (3.67×10^{-2} Pa.s), L is the liquid oil superficial flow rate (7.07×10^{-3} m/s), and $\frac{\Delta P}{\Delta Z}$ is the pressure drop per change in the reactor length (negligible due to TBR operating at atmospheric condition and short length of bed).

The liquid holdup obtained with the current optimized condition (oil flow rate of 3 mL/min) for the EBSA/AC and EBSA/LDPE:AC(1:1) are 2.46% and 2.38%, respectively, as shown in Table 7. The correlation suggests that the liquid holdup increases with the oil flow rate. It is also

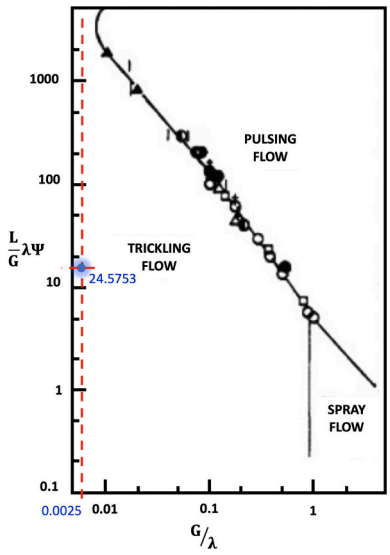

Fig. 12. Current operating regime of FFA esterification in TBR under optimized conditions *Source of map: [61].

Table 7
Liquid holdup under optimized condition.

Type of supported catalyst	Particle size, d_p (m)	Oil flow rate (mL/min)	Liquid holdup, β_d
EBSA/AC	1.00×10^{-3}	3.00	2.46%
EBSA/LDPE:AC(1:1)	1.80×10^{-3}	3.00	2.38%

seen that the FFA conversion generally increases with the liquid holdup and oil flow rate until 3 mL/min. However, as the oil flow rate increases beyond 3 mL/min, the FFA conversion drops for both types of supported catalysts. Initially, the FFA conversion increases with both the oil flow rate and liquid holdup, as this increases the residence time of the oil in the bed, which allows more FFA molecules to reach the active sites of the catalyst and react with methanol. However, above 3 mL/min, the FFA conversion decreases although the liquid holdup increases. This might be due to the buildup of stagnant oil pockets in the packed bed as the oil is retained at longer time duration. This causes a decrease in the overall utilization of catalyst particles when the oil flows continuously through the bed. Moreover, an increase in the liquid holdup could inhibit the methanol circulation in the TBR system, which might reduce the FFA reduction efficiency. Generally, EBSA/AC has a higher liquid holdup

than EBSA/LDPE:AC(1:1) due to its higher porosity and larger surface area to retain the liquid oil. (See Table 8.)

3.13.2. Catalyst wetting efficiency

Catalyst wetting efficiency is a critical component of TBRs since it significantly impacts the catalyst utilization. Internal wetting refers to the portion of the pore's surface that is covered in liquid, whereas external wetting is the portion of external catalytic surface that is covered in liquid film. Three different configurations of wetting are possible which are the partial wetting, incomplete wetting and complete wetting. The wetting efficiency can have a positive or negative effect on the reaction rate, depending on the type of reaction. If the limiting reactant is present in the liquid phase, then the reaction rates are directly proportional to the amount of catalyst wetting. Consequently, the TBR's functionality is adversely affected by the incomplete wetting. If the limiting reactants are in the gas phase, then direct interaction with the active sites is necessary. Hence, complete wetting negatively impacts the TBR's functionality. The wetting efficiency of the catalyst bed is mainly influenced by the particle size diameter and mass velocity of the liquid and gas. The wetting efficiency drops as the particle diameter increases. Eq. 10 below is the correlation proposed by Mills and Dudukovic which predicts the wetting efficiency of the catalyst bed [65].

$$\text{Wetting efficiency}, \eta_{CE} = 0.038 \cdot \dot{L}^{0.22} \cdot \dot{G}^{-0.083} \cdot d_p^{-0.373} \# \quad (10)$$

where, $\dot{L}$ is the liquid oil mass velocity (6.4723 kg/m^2.s), $\dot{G}$ is the methanol gas mass velocity (1.8248 kg/m^2.s) and d_p is the particle size (EBSA/AC: 1.00 × 10^{-3} m; EBSA/LDPE:AC(1:1): 1.80 × 10^{-3} m).

The catalyst wetting efficiency obtained from the current optimized conditions for the EBSA/AC and EBSA/LDPE:AC(1:1) are 71.70% and 57.59%, respectively. This shows that under the current optimized conditions, partial wetting takes place in the TBR for both supported catalysts. The correlation suggests that the wetting efficiency increases with the oil flow rate. It can be also seen that the FFA conversion generally increases with the wetting efficiency and oil flow rate until 3 mL/min. However, the FFA conversion drops for both types of supported catalysts as the oil flow rate increases beyond 3 mL/min. Initially, the FFA conversion increases with the oil flow rate and the wetting efficiency, as this allows for more FFA to bind onto the active sites of the catalyst and react with methanol. However, beyond 3 mL/min, the FFA conversion decreases although the wetting efficiency increases. This might be due to the higher liquid flow rate being prone to liquid maldistribution. Oil rivulets may flow unevenly over the packed bed at higher flow rate, and this leads to irregular distribution and uneven flow paths. Consequently, the oil tends to follow the path with the lowest resistance and increases the number of stagnant oil pocket and dry zones within the bed. Hence, the utilization of active sites by the reactants decreases. Moreover, higher catalyst wetting by oil reduces the direct transfer of methanol vapor to the active sites. This causes the methanol vapor to be transferred to the active sites through the oil layer, which generally has higher mass transfer resistance than the direct transfer. As a result, an optimum level of catalyst wetting efficiency must be achieved without jeopardizing the FFA conversion. Generally, EBSA/AC has higher wetting efficiency than EBSA/LDPE:AC(1:1) due its higher porosity and larger contact surface area with the flowing liquid.

Table 8
Catalyst wetting efficiency under optimized conditions.

Type of supported catalyst	Particle size, d_p (m)	Oil flow rate (mL/min)	Methanol flow rate (mL/s)	Wetting Efficiency, η
EBSA/AC	1.00 × 10^{-3}	3.00	2.41	71.70%
EBSA/LDPE:AC (1:1)	1.80 × 10^{-3}	3.00	2.41	57.59%

3.13.3. Mass transfer coefficients

Mass transfer can be categorized into gas-liquid, liquid-solid and gas-solid mass transfer. The gas-liquid mass transfer rates are affected by the particle size diameter, gas and liquid flow rates, fluid properties and reactor operating conditions. The influence of particle size diameter on the gas-liquid mass transfer rates is greater than the reactor configuration (diameter, height). In addition to the particle size, the gas and liquid throughputs have a significant impact on the gas-liquid mass transfer rates. The higher flow rates of gas and liquid enhance their interaction and increase the gas-liquid interfacial area. Eq. 11 to 16 below are the correlation proposed by Wild and Larachi for low interaction regime [66]. The gas-liquid interfacial area is calculated based on correlation suggested by Hirose and Toda [67].

For low interaction regimes:

$$\frac{k_{GL} a_{GL} d_h^2}{D_{AL}} = 2 \times 10^{-4} \left[X_G^{0.25} Re_L^{0.2} We_L^{0.2} Sc_L^{0.5} \left(\frac{a_v d_h}{1 - \varepsilon_B} \right)^{0.25} \right]^{3.4} \quad (11)$$

$$\text{Modified Lockhart} - \text{Martinelli number}, X_G = \frac{G}{L} \sqrt{\frac{\rho_G}{\rho_L}} \quad (12)$$

$$\text{Weber number of liquid phase}, We_L = \frac{L^2 d_p \rho_L}{\delta_L} \quad (13)$$

$$\text{Schmidt number of liquid phase}, Sc_L = \frac{\mu_L}{\rho_L D_{AL}} \quad (14)$$

$$\text{Hydraulic diameter}, d_h = d_p \sqrt[3]{\frac{16 \varepsilon_B{}^3}{9\pi (1 - \varepsilon_B)^2}} \quad (15)$$

$$\text{Gas} - \text{liquid interfacial area}, a_{GL} = 175 \bullet d_p{}^{-0.8} \bullet G^{0.6} \bullet L^{0.5} \# \quad (16)$$

where,

k_{GL} is the gas-liquid mass transfer coefficient (m/s), a_v is the particle surface area per unit bed volume (EBSA/AC: 1.71 × 10^7 m^{-1}, EBSA/LDPE:AC(1:1): 8.52 × 10^6 m^{-1}), a_{GL} is the gas-liquid interfacial area (EBSA/AC: 96.68 m^2, EBSA/LDPE:AC(1:1): 60.41 m^2) and D_{AL} is the diffusivity of methanol gas in liquid oil (6.00 × 10^{-7} m^2/s), L is the liquid oil superficial flow rate (7.07 × 10^{-3} m/s), G is the methanol gas superficial flow rate (0.0023 m/s), ρ_G is the density of methanol vapor (1.21 kg/m^3), ρ_L is the density of oil (915 kg/m^3), σ_L is the surface tension of oil (3.08× 10^{-2} N/m), μ_L is the viscosity of oil (3.67× 10^{-2} Pa.s), ε_B is the bed void (0.50).

The liquid-solid mass transfer rate is determined by the amount of liquid contact with an accessible solid surface. The liquid flow rate increases the wetting efficiency, which raises the liquid-solid mass transfer rates. Considering that the mass transfer rates cannot be determined without accounting for the catalyst wetting efficiency, Eq. 17 and 18 below is the correlation proposed by Chou which includes the wetting efficiency as a parameter along with the liquid-solid mass transfer coefficient [68]. Constant a and b are 1.84 and 0.48 respectively [69].

$$\eta_{CE} Sh = a \cdot Re_L{}^b \cdot Sc_L{}^{\frac{1}{3}} \# \quad (17)$$

$$\text{Sherwood number}, Sh = \frac{k_{LS} d_h}{D_{AL}} \# \quad (18)$$

where,

k_{LS} is the liquid − solid mass transfer coefficient (m/s), η_{CE} is the wetting efficiency, D_{AL} is the diffusivity in oil phase (6 × 10^{-7} m^2/s), d_p is the particle size (EBSA/AC: 1.00 × 10^{-3} m; EBSA/LDPE:AC(1:1): 1.80 × 10^{-3} m).

The gas-solid mass transfer rate is also necessary when the catalyst particles are partially wetted. The gas phase reactants and the external catalyst surface make direct contact when dry spots are present on the catalyst surface. The gas-solid mass transfer coefficient can be deter-

mined using the correlation proposed by Kiel and Prins as shown in Eq. 19 to 22 below [70].

$$\text{Sherwood number, } Sh = 2.0 + 0.6 Re_G^{\frac{1}{2}} Sc_G^{\frac{1}{3}} \# \quad (19)$$

$$\text{Sherwood number, } Sh = \frac{k_{GS} d_h}{D_{AL}} \# \quad (20)$$

$$\text{Reynolds number of gas phase, } Re_G = \frac{\rho_G G d_p}{\mu_G} \# \quad (21)$$

$$\text{Schmidt number of gas phase, } Sc_G = \frac{\mu_G}{\rho_G D_{AB}} \# \quad (22)$$

where,

k_{GS} is the gas-solid mass transfer coefficient (m/s), D_{AB} is the diffusivity of the methanol gas phase in air (1.64×10^{-5} m^2/s), G is the methanol gas superficial flow rate (0.0023 m/s), $\rho_G$is the density of methanol vapor (1.21 kg/m^3), d_p is the particle size (EBSA/AC: 1.00×10^{-3} m; EBSA/LDPE:AC(1:1): 1.80×10^{-3}, $\mu_G$is the viscosity of methanol vapor (1.14×10^{-5} Pa.s) and ε_B is the bed void (0.50).

As presented in Table 9 below, the gas-liquid mass transfer coefficients calculated using Eq. 11 for EBSA/AC and EBSA/LDPE:AC(1:1) are 8.51×10^{-4} and 1.54×10^{-3} ms^{-1}, respectively. The liquid-solid mass transfer coefficients calculated using Eq. 17 to 18 for the EBSA/AC and EBSA/LDPE:AC(1:1) are 4.14×10^{-3} and 3.80×10^{-3} ms^{-1}, respectively. Lastly, the gas-solid mass transfer coefficients calculated using Eq. 19 to 22 for the EBSA/AC and EBSA/LDPE:AC(1:1) are 5.61×10^{-2} ms^{-1} and 3.23×10^{-2} ms^{-1}, respectively, For both types of supported catalysts, the gas-liquid mass transfer is the slowest while the gas-solid mass transfer is the fastest. Faster gas-solid mass transfer indicates that when the TBR operates in the trickle flow regime where oil is the dispersed phase and methanol vapor is the continuous phase, the methanol vapor tends to flow along the pathway with the lowest resistance, which is the direct transfer to the active sites instead of using the oil layer as a medium to reach the active sites. This consequently reduces the gas-liquid mass transfer due to its higher resistance. It can be also seen that the liquid-solid and gas-solid mass transfer is faster in the EBSA/AC compared to the EBSA/LDPE:AC(1:1). This might be due to its higher catalyst wetting, lower particle size and porous structure of the AC in EBSA/AC which retains more liquid oil layer and facilitates more methanol molecule to be channeled to the active sites compared to the EBSA/LDPE:AC.

The successful design of high-performance reactors requires a deep understanding of physical transport phenomena and material science. Effective reactor performance relies on optimizing mass transfer among reactants [70]. Furthermore, the selection of reactor materials is essential for developing novel green inhibitors; understanding surface chemistry is critical to significantly improving the corrosion resistance of alloys in acidic and saline mediums [71–73]. These technical considerations are essential for scaling up next-generation fuel cell configurations and high-efficiency chemical reactors [74].

Table 9
Mass transfer coefficients under optimized conditions.

Type of supported catalyst	Particle size, d_p (m)	Gas-Liquid Mass Transfer Coefficient, k_{GL} (m/s)	Liquid-Solid Mass Transfer Coefficient, k_{LS} (m/s)	Gas-Solid Mass Transfer Coefficient, k_{GS} (m/s)
EBSA/AC	1.00×10^{-3}	8.51×10^{-4}	4.14×10^{-3}	5.61×10^{-2}
EBSA/LDPE:AC (1:1)	1.80×10^{-3}	1.54×10^{-3}	3.80×10^{-3}	3.23×10^{-2}

3.14. Mechanism of Free fatty acid esterification in trickle bed reactor

Mechanism of FFA esterification in TBR system compromises various steps of mass transfer and surface reaction which determines the overall reaction rate [27]. Step 1 is the transport of methanol molecules in gas phase to bulk liquid oil phase. Step 2 is the transport of both methanol and FFA molecules to the surface of supported catalyst, EBSA/AC and EBSA/LDPE:AC (1:1). Step 3 is the intraparticle diffusion of methanol and FFA molecules within the pore of supported catalyst. Step 4 is the adsorption of methanol and FFA molecules on the catalyst sites and surface chemical reaction of adsorbed methanol and FFA to yield FAME and water. Lastly, step 5 is the desorption of FAME and water to the bulk liquid oil phase. Fig. 13 and Fig. 14 illustrate the proposed mechanism of FFA esterification in TBR packed with EBSA/AC and EBSA/LDPE:AC (1:1), respectively.

In Fig. 13, the EBSA/AC catalyst benefits from the high surface area and well-developed pore structure of AC, which facilitates efficient mass transfer and diffusion of methanol and FFA to the catalytic sites. The accessible pores and abundant active sites ensure rapid adsorption, surface reaction, and desorption of the products (FAME and water). Among all tested catalysts, EBSA/AC achieved the highest FFA conversion and the lowest catalyst consumption. This highlights the superior catalytic efficiency and optimal utilization of the active phase due to the favourable physical characteristics of AC.

In Fig. 14, the incorporation of LDPE into the support structure introduces hydrophobicity, which aids in the continuous removal of water, a by-product that can inhibit the acid-catalyzed reaction. However, the presence of LDPE also partially obstructs the pores and reduces the effective surface area of activated carbon, limiting the access of reactants to the active sites. Consequently, while EBSA/LDPE:AC(1:1) still demonstrated high catalytic activity and acceptable FFA conversion, it was slightly less efficient compared to EBSA/AC and required a higher catalyst consumption for similar performance.

EBSA/AC catalyst remains the most efficient in terms of both conversion and catalyst economy, making it a more favourable choice for FFA esterification in TBR.

4. Conclusions

In this study, EBSA catalyst was supported on LDPE and AC hybrid with 5 different mass ratios and these supported acid catalysts were used to perform esterification of ACPO with a FFA content of 10.17 wt% using TBR. Characterization of the supported catalysts were done, and results show that the EBSA was well impregnated on both AC and LDPE:AC(1:1) supports. All experiments were conducted in counter-current mode due to its higher conversion in comparison with co-current mode. EBSA/AC

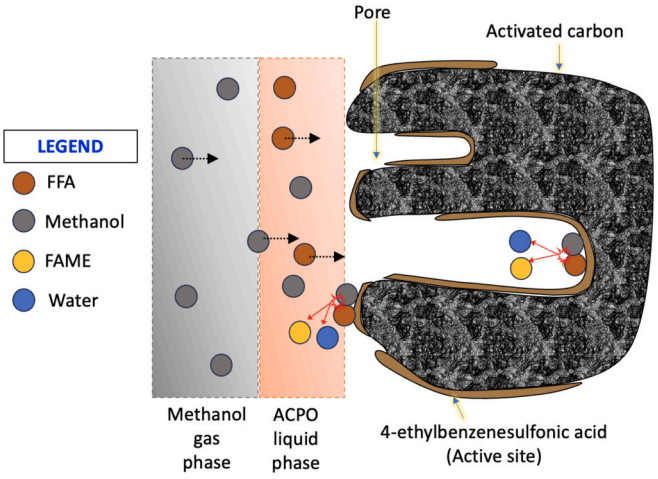

Fig. 13. Mechanism of FFA esterification in TBR packed with EBSA/AC.

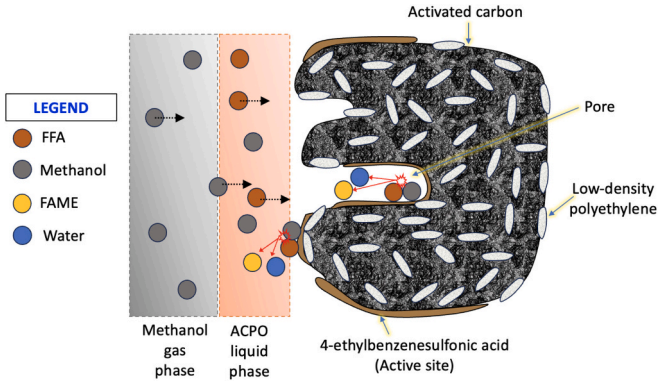

Fig. 14. Mechanism of FFA esterification in TBR packed with EBSA/LDPE: AC(1:1).

achieved the highest yield of treated ACPO and the lowest catalyst consumption since it can be recycled for 3 times under the following optimum conditions: 14 g of EBSA catalyst impregnated onto 6 g of AC, oil flow rate of 3 mL/min, 50 mL of methanol fed to the reboiler, reaction temperature of 65 °C. It was found that TBR was operated under the trickle flow regime and hydrodynamic parameters such as liquid holdup, catalyst wetting efficiency, liquid-solid mass transfer coefficient and gas-solid mass transfer coefficients were higher for EBSA/AC compared to EBSA/LDPE:AC(1:1). Overall, the optimization and hydrodynamics studies highly recommended to apply EBSA/AC without LDPE to gain high yield of treated oil and achieve better hydrodynamics. However, this study shows the feasibility and potential use of polyethylene-activated carbon hybrid supported catalyst for continuous FFA esterification.

Having said that, several limitations should also be considered. Firstly, current study focused primarily on the initial stage of esterification, using hydrodynamic parameters derived from raw material properties. Secondly, current study may not fully capture the complexities of industrial-scale operations which includes fluctuating incoming properties, scale-dependent hydrodynamics and fouling behavior. Thirdly, long-term stability and regeneration potential of catalyst were not extensively investigated. Understanding catalyst lifespan is essential for ensuring cost-effectiveness and sustainability.

Addressing these limitations in future studies would further strengthen the practical relevance and applicability of this catalytic system. This can be done through scale-up studies to industrial scale to validate reactor performance under real process conditions, studies on catalyst stability and regeneration to assess the long-term performance and reusability of supported catalysts and life cycle assessment and techno-economic analysis (TEA) to evaluate environmental effect and financial viability at a commercial scale.

CRediT authorship contribution statement

Prabakaran Uthamaseelan: Writing – original draft, Investigation. **Adeeb Hayyan:** Writing – review & editing, Supervision, Conceptualization. **Mahar Diana Hamid:** Writing – review & editing, Supervision. **Khalid M. Abed:** Writing – review & editing, Data curation. **Jehad Saleh:** Writing – review & editing. **Barun Kumar Chakrabarti:** Writing – review & editing. **Bhaskar Sen Gupta:** Writing – review & editing. **Wan Jefrey Basirun:** Writing – review & editing. **Zulhelmi Amir:** Writing – review & editing. **M. Zulhaziman M. Salleh:** Writing – review & editing. **Yousef Mohammed Alanazi:** Writing – review & editing, Funding acquisition.

Declaration of competing interest

The authors declare that they have no known competing financial interests or personal relationships that could have appeared to influence the work reported in this paper.

Acknowledgements

This work was financially supported by the Ministry of Higher Education, Malaysia, for niche area research under the Higher Institution Centre of Excellence (HICoE) program (JPT(BKPI)1000/016/018/28 Jld.3(2) & NANOCAT-2024B). The authors would like to acknowledge the financial support from Ongoing Research Funding program, (ORF-2026-511), King Saud University, Riyadh, Saudi Arabia.

Data availability

Data will be made available on request.

References

[1] N. Dian, et al., Palm oil and palm kernel oil: versatile ingredients for food applications, J. Oil Palm Res. 29 (4) (2017) 487–511.
[2] A.Q. Abdul-Hamid, M.H. Ali, L.H. Osman, M.L. Tseng, The drivers of industry 4.0 in a circular economy: The palm oil industry in Malaysia, Journal of Cleaner Production 324 (2021) 129216, https://doi.org/10.1016/j.jclepro.2021.129216.
[3] S.K. Mishra, P.D. Belur, R. Iyyaswami, Use of antioxidants for enhancing oxidative stability of bulk edible oils: a review, Int. J. Food Sci. Technol. 56 (1) (2021) 1–12.
[4] A.F.A. Nizam, M.S. Mahmud, Food quality assurance of crude palm oil: a review on toxic ester feedstock, OCL 28 (2021) 23.
[5] M.E. Di Pietro, A. Mannu, A. Mele, NMR determination of free fatty acids in vegetable oils, Processes 8 (4) (2020) 410.
[6] K.A. Zahan, M. Kano, Biodiesel production from palm oil, its by-products, and mill effluent: a review, Energies 11 (8) (2018) 2132.
[7] N. Puagsang, et al., Production of biodiesel from low-grade crude palm oil using hydrochloric acid, EnvironmentAsia 14 (1) (2021).
[8] P. Muanruksa, J. Winterburn, P. Kaewkannetra, A novel process for biodiesel production from sludge palm oil, MethodsX 6 (2019) 2838–2844.
[9] I. Satar, W.N.R. Wan Isahak, J. Salimon, Characterization of biodiesel from second generation gamma-irradiated *Jatropha curcas*, Journal of the Taiwan Institute of Chemical Engineers 49 (2015) 85–89, https://doi.org/10.1016/j.jtice.2014.10.026.
[10] T. Changwatchai, et al., Separation of free fatty acid and triglycerides by molecular distillation–experimental and simulation approaches, Processes 10 (10) (2022) 2053.
[11] T. Zhang, K. Shahbaz, M.M. Farid, Glycerolysis of free fatty acid in vegetable oil deodorizer distillate catalyzed by phosphonium-based deep eutectic solvent, Renew. Energy 160 (2020) 363–373.
[12] D. Yu, et al., Enzymatic esterification of rice bran oil and phytosterol in supercritical CO2, J. Food Process. Preserv. 43 (9) (2019) e14066.
[13] M. Veillette, et al., Esterification of free fatty acids with methanol to biodiesel using heterogeneous catalysts: from model acid oil to microalgae lipids, Chem. Eng. J. 308 (2017) 101–109.
[14] E.L. Almeida, C.M.G. Andrade, O.A. dos Santos, Production of biodiesel via catalytic processes: a brief review, Int. J. Chem. React. Eng. 16 (5) (2018).
[15] A.N. Masri, et al., Rapid esterification of fatty acid using dicationic acidic ionic liquid catalyst via ultrasonic-assisted method, Ultrason. Sonochem. 60 (2020) 104732.
[16] N. Mansir, et al., Investigation of heterogeneous solid acid catalyst performance on low grade feedstocks for biodiesel production: a review, Energy Convers. Manag. 141 (2017) 171–182.
[17] S.F. Ibrahim, N. Asikin-Mijan, M.L. Ibrahim, G. Abdulkareem-Alsultan, S.M. Izham, Y.H. Taufiq-Yap, Sulfonated functionalization of carbon derived corncob residue via hydrothermal synthesis route for esterification of palm fatty acid distillate, Energy Conversion and Management 210 (2020) 112698, https://doi.org/10.1016/j.enconman.2020.112698.
[18] P. Kutálek, et al., Aspects of Mg–Al mixed oxide activity in transesterification of rapeseed oil in a fixed-bed reactor, Fuel Process. Technol. 122 (2014) 176–181.
[19] J.I. Orege, et al., Recent advances in heterogeneous catalysis for green biodiesel production by transesterification, Energy Convers. Manag. 258 (2022) 115406.
[20] N. Singh, et al., Progress and facts on biodiesel generations, production methods, influencing factors, and reactors: a comprehensive review from 2000 to 2023, Energy Convers. Manag. 302 (2024) 118157.
[21] W. Jindapon, et al., Continuous production of fatty acid methyl esters and high-purity glycerol over a dolomite-derived extrudate catalyst in a countercurrent-flow trickle-bed reactor, Renew. Energy 157 (2020) 626–636.
[22] J. Hanika, et al., Multi-functional trickle bed reactor for butylacetate synthesis, Catal. Today 79 (2003) 83–87.
[23] M.R. Parvizi, M. Ardjmand, S. Habibzadeh, Elucidation of the effect of TiO2 in the synthesized nanocatalyst of Co–Mo@ Al2O3–TiO2 for the hydrogenation of C6–C8 olefins, Catal. Lett. (2023) 1–12.
[24] C.E. Ramírez-Castelán, et al., Mathematical modelling and simulation of a trickle-bed reactor for hydrotreating of petroleum feedstock, Int. J. Chem. React. Eng. 17 (7) (2019) 20180176.

[25] Biardi, G. and G. Baldi, Three-phase catalytic reactors. Catal. Today, 1999. 52 (2–3): p. 223–234.
[26] G. Wehinger, et al., Instabilities in fixed bed reactors with downwards directed flow for the oligomerization of 1-Butene, Chem. Ing. Tech. 94 (5) (2022) 663–670.
[27] V.V. Ranade, R. Chaudhari, P.R. Gunjal, Trickle bed reactors: Reactor engineering and applications, Elsevier, 2011.
[28] L. Gehrke, et al., Structural and energetic characterization of silica-alumina gels for adsorption processes, Microporous Mesoporous Mater. 365 (2024) 112891.
[29] A. Vieira Coelho, et al., Specific surface area and structures of aluminas from fibrillar pseudoboehmite, Matéria (Rio de Janeiro) 13 (2008) 329–341.
[30] R. Bamidele, M. Marszewski, Carbonization and activation of lignocellulosic biomass in liquid phase at sub-200° c temperatures, ACS Sustain. Chem. Eng. (2025).
[31] M. Sankar, et al., Role of the support in gold-containing nanoparticles as heterogeneous catalysts, Chem. Rev. 120 (8) (2020) 3890–3938.
[32] T.W. Chew, et al., A review of bio-based activated carbon properties produced from different activating chemicals during chemicals activation process on biomass and its potential for Malaysia, Materials 16 (23) (2023) 7365.
[33] Y. Lee, et al., Biochar as a catalytic material for the production of 1, 4-butanediol and tetrahydrofuran from furan, Environ. Res. 184 (2020) 109325.
[34] N. Jagadeesh, B. Sundaram, Adsorption of pollutants from wastewater by biochar: a review, J. Hazardous Mater. Adv. 9 (2023) 100226.
[35] J. Huang, et al., Chemical recycling of plastic waste for sustainable material management: a prospective review on catalysts and processes, Renew. Sust. Energ. Rev. 154 (2022) 111866.
[36] G. Tatrari, et al., Waste plastic derived graphene sheets as nanofillers to enhance mechanical strength of concrete mixture: an inventive approach to deal with universal plastic waste, Cleaner Eng. Technol. 5 (2021) 100275.
[37] O. Olofinnade, et al., Solid waste management in developing countries: Reusing of steel slag aggregate in eco-friendly interlocking concrete paving blocks production, Case Stud. Constr. Mater. 14 (2021) e00532.
[38] E. Valadez-Renteria, et al., Flexible CuS/TiO2 based composites made with recycled bags and polystyrene for the efficient removal of the 4-CP pesticide from drinking water, Sep. Purif. Technol. 270 (2021) 118821.
[39] M.M.d.M.S. Moura, et al., Degradation of the mixture of the ketoprofen, meloxicam and tenoxicam drugs using TiO2/metal photocatalysers supported in polystyrene packaging waste, Water Sci. Technol. 83 (4) (2021) 863–876.
[40] J. Bartáček, et al., Recoverable polystyrene-supported catalysts for sharpless allylic alcohols epoxidations, React. Funct. Polym. 137 (2019) 123–132.
[41] A. Mossmann, et al., Preparation of polyethylene–supported zero–valent iron buoyant catalyst and its performance for ponceau 4R decolorization by photo–Fenton process, J. Environ. Chem. Eng. 7 (2) (2019) 102963.
[42] S. Sandhu, et al., Photocatalytic denitrification of water using polystyrene immobilized TiO2 as floating catalyst, J. Environ. Chem. Eng. 8 (6) (2020) 104471.
[43] Q. Zhang, et al., Biochar filled high-density polyethylene composites with excellent properties: towards maximizing the utilization of agricultural wastes, Ind. Crop. Prod. 146 (2020) 112185.
[44] Q. Zhang, et al., Mussel-inspired polydopamine-modified biochar microsphere for reinforcing polylactic acid composite films: Emphasizing the achievement of excellent thermal and mechanical properties, Int. J. Biol. Macromol. 260 (2024) 129567.
[45] J. Chen, et al., Achieving the simultaneous improvement of degradation, thermal, and mechanical properties of polylactic acid composite films by carbon quantum dots, Compos. Part B Eng. 299 (2025) 112442.
[46] J. Ren, et al., All-biomass derived nanocomposite films, Nano Lett. 25 (19) (2025) 7810–7817.
[47] J. Ren, et al., All-biomass nanocomposite films via facile and sustainable design procedure for thermal management and electromagnetic interference shielding, Adv. Sci. 12 (43) (2025) e10372.
[48] G. Yassaghi, et al., Preparation, characterization and first application of aerosil silica supported acidic ionic liquid as a reusable heterogeneous catalyst for the synthesis of 2, 3-dihydroquinazolin-4 (1H)-ones, Bull. Korean Chem. Soc. 33 (8) (2012) 2724–2730.
[49] L.A. Anderson, A.K. Franz, Real-time monitoring of transesterification by 1H NMR spectroscopy: Catalyst comparison and improved calculation for biodiesel conversion, Energy Fuel 26 (10) (2012) 6404–6410.
[50] S. Behzadi, M.M. Farid, Production of biodiesel using a continuous gas–liquid reactor, Bioresour. Technol. 100 (2) (2009) 683–689.
[51] H. Zhang, et al., Esterification of fatty acids from waste cooking oil to biodiesel over a sulfonated resin/PVA composite, Cat. Sci. Technol. 6 (14) (2016) 5590–5598.
[52] Y.-L. Meng, et al., Transesterification of rapeseed oil for biodiesel production in trickle-bed reactors packed with heterogeneous ca/Al composite oxide-based alkaline catalyst, Bioresour. Technol. 136 (2013) 730–734.
[53] S.M. Son, K. Kusakabe, Transesterification of sunflower oil in a countercurrent trickle-bed reactor packed with a CaO catalyst, Chem. Eng. Process. Process Intensif. 50 (7) (2011) 650–654.
[54] U. Zia, et al., Integrating environmental remediation with biodiesel production from toxic non-edible oil seeds (croton bonplandianus) using a sustainable phyto-nano catalyst, Biomass Bioenergy 190 (2024) 107406.
[55] A. Hayyan, et al., The development of new homogenous and heterogeneous catalytic processes for the treatment of low grade palm oil, J. Mol. Liq. 344 (2021) 117574.
[56] M. Otadi, et al., Reduction of free fatty acids of waste oil by acid-catalyzed esterification, Procedia Eng. 18 (2011) 168–174.
[57] A.J. Fletcher, Y. Uygur, K.M. Thomas, Role of surface functional groups in the adsorption kinetics of water vapor on microporous activated carbons, J. Phys. Chem. C 111 (23) (2007) 8349–8359.
[58] S.M. Son, H. Kimura, K. Kusakabe, Esterification of oleic acid in a three-phase, fixed-bed reactor packed with a cation exchange resin catalyst, Bioresour. Technol. 102 (2) (2011) 2130–2132.
[59] K. Singh, S.P. Kumar, B. Blümich, Monitoring the mechanism and kinetics of a transesterification reaction for the biodiesel production with low field 1H NMR spectroscopy, Fuel 243 (2019) 192–201.
[60] A. Attou, C. Boyer, G. Ferschneider, Modelling of the hydrodynamics of the cocurrent gas–liquid trickle flow through a trickle-bed reactor, Chem. Eng. Sci. 54 (6) (1999) 785–802.
[61] J.C. Charpentier, M. Favier, Some liquid holdup experimental data in trickle-bed reactors for foaming and nonfoaming hydrocarbons, AICHE J. 21 (6) (1975) 1213–1218.
[62] H. Bouras, Prediction of Mass Transfer Performances in Trickle-Bed Reactors Equipped with Innovative Catalyst Shapes, Université de Lyon, 2021.
[63] M. Al-Herz, Multiphase Catalytic Reactions in a Trickle Bed Reactor, University of Birmingham, 2012.
[64] W. Wammes, S. Mechielsen, K. Westerterp, The influence of pressure on the liquid hold-up in a cocurrent gas-liquid trickle-bed reactor operating at low gas velocities, Chem. Eng. Sci. 46 (2) (1991) 409–417.
[65] P. Mills, M. Dudukovic, Evaluation of liquid-solid contacting in trickle-bed reactors by tracer methods, AICHE J. 27 (6) (1981) 893–904.
[66] G. Wild, F. Larachi, J. Charpentier, Heat and Mass Transfer in Gas-Liquid-Solid Fixed Bed Reactors, Elsevier, Amsterdam, The Netherlands, 1992.
[67] T. Hirose, M. Toda, Y. Sato, Liqusd phase mass transfer in packed bed reactor with cocurrent gas-liquid downflow, J. Chem. Eng. Jpn 7 (3) (1974) 187–192.
[68] T.S. Chou, F.L. Worley Jr., D. Luss, Local particle-liquid mass transfer fluctuations in mixed-phase cocurrent downflow through a fixed bed in the pulsing regime, Ind. Eng. Chem. Fundam. 18 (3) (1979) 279–283.
[69] G.B. Delaunay, et al., Electrochemical determination of liquid-solid mass transfer in fixed bed irrigated gas-liquid reactor with downward co-current flow, Int. Chem. Eng. 22 (1982) 244–251.
[70] J. Kiel, W. Prins, W.P.M. van Swaaij, Mass transfer between gas and particles in a gas—solid trickle flow reactor, Chem. Eng. Sci. 48 (1) (1993) 117–125.
[71] N.A.M. Radzuan, The influence of temperature and electrophoresis deposition green inhibitor on bipolar plate AA5052 in sulfuric acid medium, Sains Malaysiana 49 (11) (2020) 3169–3177.
[72] M.S. Dania, I.B. Davea, A. Josephb, Improvement in corrosion resistance of magnesium-aluminum alloy via friction stir processing, Jurnal Kejurutera. 33 (4) (2021) 1037–1044.
[73] S. Yahya, A.A. Rahim, A.M. Shah, R. Adnan, Inhibitive behaviour of corrosion of aluminium alloy in NaCl by mangrove tannin, Sains Malaysiana 40 (9) (2011) 953–957.
[74] N.S. Hazri, S. Basri, A.M. Zainoodin, M.M. Ahmad, S.K. Kamarudin, Tuning magnesium-air fuel cell performance and corrosion behavior through electrode and electrolyte configuration, Jurnal Kejuruteraan 37 (2) (2025) 271–285.